BOLETIN DE LA SOCIEDAD ESPAÑOLA DE
Cerámica y Vidrio
www.elsevier.es/bsecv

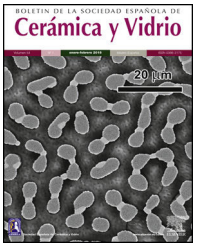

Laser processing of ceramic materials for electrochemical and high temperature energy applications

Rosa I. Merino[a,*], *Miguel A. Laguna-Bercero*[a], *Ruth Lahoz*[a], *Ángel Larrea*[a], *Patricia B. Oliete*[a], *Alodia Orera*[a], *José I. Peña*[a], *María Luisa Sanjuán*[a], *Daniel Sola*[b]

[a] *Instituto de Nanociencia y Materiales de Aragón, CSIC-Universidad de Zaragoza, 50009 Zaragoza, Spain*
[b] *Aragonese Foundation for Research and Development (ARAID), Government of Aragon, 50018 Zaragoza, Spain*

ARTICLE INFO

Article history:
Received 29 June 2021
Accepted 17 September 2021
Available online 23 October 2021

Keywords:
Laser processing
Ceramics
Selective laser melting
Laser machining
Eutectic oxides
Solid oxide cells
Selective emitters

ABSTRACT

The laser is a powerful tool for materials processing, incorporated already in many industrial processes and laboratory procedures. In this work, we are concerned with laser processing applied to research and development of ceramics for electrochemical cells and other high temperature oxide ceramics for energy applications. Solidification of single crystals or composites of relevant oxides can be performed by the laser assisted floating zone method, providing samples for structural, mechanical or functional fundamental research, as well as knowledge about its manufacture by melt processes. Selective laser melting of these ceramic oxides is a very promising technology, at the research level. Successful examples of surface laser melting of oxide eutectic composites are presented. The technologies of subtractive laser processing of ceramics (cutting, drilling, structuring, cleaning, etc.) are more developed, and the research is directed towards the optimization of mechanisms, increase of resolution and efficiency and the investigation of the effects of the laser treatment on the functional performance. Different laser processes of SOC (solid oxide cell) components are shown to decrease the ohmic, concentration and activation losses. The manuscript describes the state-of-the art of the technologies as applied to oxide and composite materials present in solid oxide electrochemical devices (SOFC, SOEC, and batteries) and selective emitters for thermophotovoltaics, with emphasis on the last achievements by the authors team.

* *Corresponding author.*
E-mail address: rmerino@unizar.es (R.I. Merino).
https://doi.org/10.1016/j.bsecv.2021.09.007

Procesamiento con láser de materiales para aplicaciones energéticas en dispositivos electroquímicos y de alta temperatura

Palabras clave:
Procesamiento por láser
Cerámica
Fusión selectiva por láser
Mecanizado por láser
Óxidos eutécticos
Celdas de óxido sólido
Emisores selectivos

RESUMEN

El láser es una potente herramienta para el procesamiento de materiales, incorporada ya en muchos procesos industriales y procedimientos de laboratorio. En este trabajo nos ocupamos del procesamiento láser aplicado a la investigación y desarrollo de cerámicas para celdas electroquímicas y otras cerámicas de óxido de alta temperatura para aplicaciones energéticas. La solidificación de monocristales o composites de óxidos relevantes se puede realizar mediante el método de zona flotante asistida por láser, proporcionando muestras para investigación básica estructural, de propiedades mecánicas o funcionales, así como conocimiento sobre su fabricación mediante procesos de fusión. La fusión selectiva por láser de estos óxidos cerámicos es una tecnología muy prometedora, cuyo desarrollo es todavía incipiente. Se presentan ejemplos exitosos de fusión por láser de superficie de compuestos eutécticos de óxidos. Las tecnologías sustractivas de procesamiento de cerámicas con láser (corte, taladrado, estructuración, limpieza, etc.) están más desarrolladas, y la investigación se dirige hacia la optimización de procedimientos, aumento de resolución y eficiencia y la investigación de los efectos del tratamiento láser sobre el rendimiento funcional. Diferentes procesos láser de los componentes de celda de óxido sólido disminuyen las pérdidas óhmicas, de concentración y de activación. El manuscrito describe el estado actual de las tecnologías aplicadas a óxidos y materiales compuestos presentes en dispositivos electroquímicos de óxidos sólidos (SOFC, SOEC y baterías) y emisores selectivos para aplicaciones termofotovoltaicas, con énfasis en los últimos logros del equipo.

Introduction

Lasers are ubiquitous tools in nowadays manufacturing technologies [1]. Their ample application range resides in their unique combination of versatility and automation capabilities. A laser beam is a coherent electromagnetic radiation that with optical elements can be delivered to the place where the processing is to be carried out through the air, the vacuum or appropriate robust optical fibres. If required, it can also be sharply focused in volumes of the order of some μm^3. There are lasers with wavelengths from the far infrared (FIR) to the ultraviolet (UV) range of the spectrum, continuous wave (CW) or pulsed with pulse duration from milliseconds to femtoseconds, and delivering average powers from μW to kW. Monochromaticity, coherence length and modal composition can also be chosen to adapt to the intended application [2].

When the laser light reaches the material it is absorbed, exciting the electronic and phonon subsystems in most of the material processing procedures through multiphoton, high order processes. In the end this produces a fast local temperature rise that can heat, melt or vaporize the material. The vapour will also interact with the incoming laser radiation and other chemical or mechanical effects come also together. The laser operation regime and the material properties determine which are the dominant processes taking place, and so one speaks of heating, melting or ablation, as the processing mechanisms.

Technologically, one of the most interesting aspects of laser processing is that it allows the total automation and flexibility of production processes, owing to, above all, its ability to be controlled in its fundamental parameters (speed, size and shape of beam, energy per pulse and power) and the requirement of minimal material handling. This allows a very precise control of the depth, the extension and also the evolution of the temperature in the region affected by the laser irradiation, which can also be monitored. This excellent adaptability offers procedures of materials surface processing with high added value and in a respectful way with the environment, as it is a chemically clean process. No chemicals or massive waste products are generated when laser treating materials. All these properties have an impact in material processing applications as they translate into high processing rates and low costs.

One example of the versatility and environmental friendliness of lasers can be found in their application in the cleaning of materials of cultural interest [3]. Decontamination techniques have been based on the direct application of chemical products, different forms of washing, and mechanical cleaning processes [4,5]. However, in addition to cleaning, these techniques cause a significant environmental impact and pose a risk to the health of the operator, as well as generally causing significant variations in the composition and structure of the treated surfaces. Avoiding these drawbacks, laser cleaning can be used to eliminate corrosion patina on metals [6], organic paints on granites or weathering dirt on ancient brick masonry such as Mudéjar Architectonic Art [7], which encompass a variety of compositions. This last application combines the challenge of cleaning with the application to massive surfaces. This also requires working on the development of combined systems and laser characterization cleaning stations for the conservation of large monumental surfaces that allow a real

-time analysis of the surface to determine the degree of cleaning carried out and when the process should stop.

Lasers have today very diverse applications in materials processing and are widely incorporated into industry [1]. They have been developed and researched for ceramic processing too. In the present work we will review its present use and perspectives in the processing of the ceramics involved in oxide electrochemical devices and other high temperature oxide composites for energy. We will discuss its use in several processing of ceramics for energy from our own experience.

Melting and solidification

Solidification of oxides and composite materials. The LFZ method

Single crystals or strongly textured materials are required in many applications, as high quality semiconductors in photovoltaics, for optical applications or complex oxides such as for example thermoelectric ceramics for energy harvesting [8]. Other times crystals are required to perform basic research on materials of technological relevance [9–12]. There are well established procedures for crystal growth for research as well as for industrial processes [13]. The crystallization processes are quite complex as they involve different phases (solid crystal, melt or solution and vapour phases), heat and material transport in different length scales as well as thermomechanical constrains. Different procedures are appropriate for different compounds and crystal sizes. In the present section, we are focused on the use of lasers to assist the solidification of materials from a melt. The laser is then used to heat the material, if possible with minimal or controlled evaporation, up to melting, which followed by a controlled cooling process gives rise to single crystals, glasses or composites, as required.

The laser floating zone (LFZ) solidification method is a directional solidification process that relies on melting a small volume of material using a laser as the heating source [14]. It is also termed laser heated pedestal growth (LHPG). It is equivalent to solidification in an arc-image furnace in the sense that both methods use light as the energy source for heating and that the melt is held by surface tension forces. An image of the light source is formed on the material to melt using appropriate optical elements. Fig. 1 shows the experimental layout at our laboratory [15]. It consists of a CW CO_2 semi-sealed laser of 600 W (Electronic Engineering, Firenze, Blade 600, $\lambda = 10.6\ \mu m$), an in-house built growth chamber with gold coated metal mirrors for beam focussing and two vertical axes for the rod displacement. Both axes have independent rotation and translation movement. The beam is annularly shaped with the help of a reflaxicon, focused on the lower end of a sintered rod of material, the feedstock. A drop of molten material is formed, a seed on which the solidification is to start is pushed into the hot volume until a liquid bridge between the precursor and seed is established. The solidification takes place by pulling the seed out the hot region at the same time that the feedstock is pushed into the hot volume, maintaining a constant molten volume. This small molten volume is held in place by surface tension, whereby stable solidification is possible when appropriate ratios in the melt length, diameter

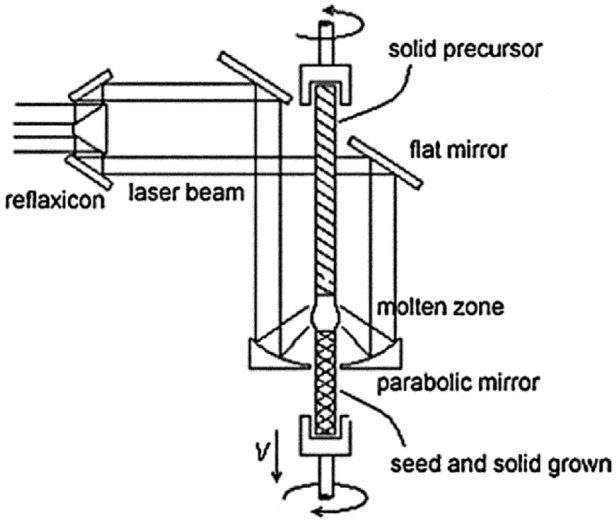

Fig. 1 – Experimental layout of the LFZ system for crystal growth.

and travelling rate, liquid viscosity and surface tension are established. Large thermal gradients (close to 10^6 K/m) are produced at the solid–liquid interface [16].

The most relevant, specific characteristics of this solidification procedure is the absence of crucible in contact with the melt, the possibility of large thermal gradients at the solid–liquid interphase, thereby allowing relatively fast solidification rates staying within the coupled eutectic solidification range, and the possibility of processing from the melt materials with high melting temperatures with relatively low energy consumption. It uses a seed to start the solidification, so it allows the use of oriented crystalline seeds to promote specific crystal orientations or glass seeds to hinder crystallization. Moreover, it is simple to control the processing atmosphere, and systems to work under relative pressure [17] or with other intervening fields (such as electric fields) have also been designed and tested. These external fields can drive the distribution of the chemical elements in the liquid and solid [18], or help to manage the flow in the melt [19]. The technique is well suited for the solidification of crystal fibres for industrial production and for research [20–22].

Large thermal gradients set up during growth and across the melt give rise to strong buoyancy, thermosolutal and Marangoni convection currents which have an impact on the solute distribution. Forced convection is often used to homogenize the heating or to compensate convection at the solidifying interface. Local overheating of the melt can also accelerate volatilization of components in some cases. The thermal gradients in the solidified crystal can also generate cracking that has to be conveniently managed for successful growth [23,24]. Computer simulations have helped to understand and harness the contribution of each technical parameter to the solidification process [25].

Oxides for electrochemical energy applications

The technique has been used in many research laboratories to produce different materials. In a recent compilation by F. Rey-García et al. [8] one can find how LFZ has been

used for solidification of many complex oxides. The technique [26] has allowed G.F. de la Fuente and coworkers from the INMA to study the physics of the transport properties of textured polycrystalline rods or fibres for technological applications (high temperature superconductors or thermoelectric oxides) over the last 20 years. If we restrict to oxides which are relevant for electrochemical devices, we have to move to ion or mixed conductors. High temperature electrolytes such as yttria stabilized zirconia (YSZ) can also be solidified from a melt. YSZ is the reference and state of the art solid electrolyte in solid oxide fuel cells and solid oxide electrolysers operating at high temperatures (above 700 °C), because it has a quite good ionic conductivity, wide electrolytic domain, excellent mechanical properties and mature state of technological development. YSZ single crystals are industrially produced at large scale using the skull-melting method and have uses based on its excellent optical and mechanical properties. At lower volumes of material and for research purposes, Prof. E.E. Lomonova and colleagues in Moscow, using solidification in a cold-crucible, have pursued recently a thorough research of optical properties (namely lasing), stability of solid solutions and ionic conductivity [27,28]. The latter complement the broad knowledge reached by the research community using skull melting produced crystals and ceramic (polycrystalline) materials as research samples. The LFZ procedure is also suitable for the solidification of stabilized zirconia, and so it was used to solidify fibres up to 200 μm diameter or rods up to 2 mm diameter of Er_2O_3 stabilized ZrO_2 to supply samples for fundamental mechanical characterization [29,30] or to fabricate samples of YSZ doped with different optically active ions for spectroscopic studies [31].The optical properties of YSZ doped with many optically active ions have also been studied over the years, with emphasis on lasing, spectroscopic probes of the defect structure or of the probes to monitor the oxygen activity [32,33]. Recently, using on-purpose LFZ solidified Terbium doped YSZ crystals, we have identified the redox couple Tb^{4+}/Tb^{3+}, candidate for oxygen activity monitoring in the high oxygen partial pressure side that might develop in SOEC devices upon operation conditions [34].

Other electrolytes were also grown by the LFZ method. Proton conducting oxides, such as doped $BaCeO_3$, $SrCeO_3$, $SrZrO_3$, $SrTiO_3$ or $Sr_3CaNb_2O_9$ were solidified for the purpose of studying their structural, mechanical and ion conducting properties [35–37]. The materials showed a textured, cellular microstructure with grains composed of the main phase (sometimes with nanodomains) and intergrain boundary areas. The conductivity was consistent with the values obtained in ceramic samples. Lithium ion conductors of $La_{2/3-x}Li_{3x}TiO_3$ (LLTO) type with perovskite structure were also solidified using the LFZ method [38]. $La_{0.5}Li_{0.5}TiO_3$ is a complex system to solidify because of lithium volatilization and phase segregation. The grown material consisted of long single-crystal grains of a major perovskite phase, although with lithium content lower than the nominal one, surrounded by rutile-TiO_2 precipitates and eutectic regions formed by a lithium-rich LLTO perovskite plus a $Li_xTi_yO_z$ oxide. Recently, Maruyama et al. [39] achieved solidification of a single phase $La_{2/3-x}Li_{3x}TiO_3$ with an IR heating image furnace and using the travelling solvent floating zone method, and obtained 5 mm diameter, 37 mm long crystals.

The LFZ technique has been applied to the production of mixed oxides of the systems CeO_x/ZrO_2 (CZO) and PrO_x/ZrO_2 (PZO), to investigate them as oxygen storage compounds in three-way-catalysts. In these systems, the high temperatures inherent to the LFZ technique allow exploring regions of the phase diagrams just below the melting temperatures, which are difficult to attain by other techniques. At those temperatures a complex interplay occurs between order/disorder processes and redox effects of the mixed-valent cerium and praseodymium cations. The feasibility of controlling parameters such as atmosphere (pO_2) and cooling rate has enabled to establish the correlation between the degree of cation ordering and the processing atmosphere in the CZO system [40]. In the PZO system we have studied the stability of the pyrochlore phase as a function of the cation and oxygen stoichiometry in different processing atmospheres [41].

Another class of ceramic materials produced by solidification, and particularly by laser assisted solidification, are directionally solidified eutectic ceramics (DSECs). The interest in those started in the seventies decade of the 20th century, mainly because of their excellent mechanical properties. They surpassed the mechanical performance of conventional ceramics due to their homogenous and fine microstructure, with clean interphase boundaries; and the one of the single crystals owing to their composite nature (two or three different phases present). Several good reviews exist on the subject [42,23], dealing with the solidification mechanisms and procedures [43], with the relationship between mechanical properties and microstructure [23,44] or related to specific applications or properties [45,46]. In parallel, and with the advancement of computational capabilities, many phase equilibrium diagrams of the relevant components have been calculated [47,48]. More recently, great interest has also been devoted to ultrahigh-temperature ceramics which, often formulated at a eutectic composition, can also be fabricated by melting procedures [49].

Already very early, the microstructure of the solidified eutectics inspired the imagination to harness functional properties of the materials [50]. More recently, properties of eutectic ceramics as biomaterials [51], metamaterials [52–54], scintillators [55], waveguide plates [56], infrared windows [57], superconductors [12] or anodes in photoelectrochemical reactors [58] rely on the specific microstructure and microstructural size of the eutectic; others such as white light emitters [59] or thermal emitters [60] take also benefit of the excellent mechanical properties. The functionalities involved in the materials for energy applications hold preeminent interest today. It is worth to remind that the LFZ method imposes a sharp thermal gradient at the solid liquid interface (of the order of 10^3 K/mm), a requirement for the coupled solidification of eutectics at large solidification rates, and thus producing homogeneous microstructures with submicrometre phase size, not attainable by other solidification methods.

Eutectic ion and mixed conductors: electrolytes and electrodes

The good mechanical properties of DS eutectic composites have prompted the study of their ion or mixed conducting properties, mainly in the ones that contain doped zirconia. Some examples are YSZ-Al_2O_3, MgSZ-MgO, CaSZ-$CaZrO_3$

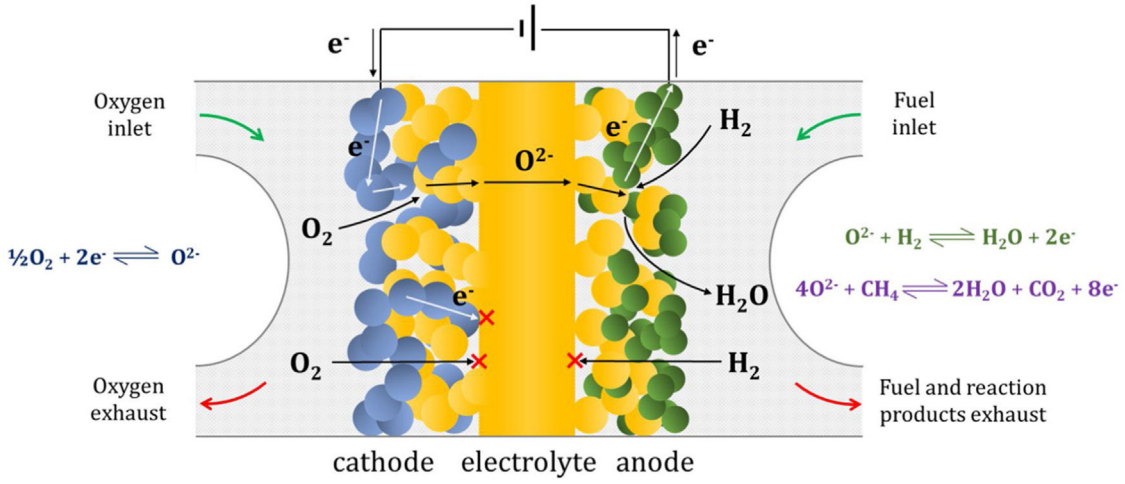

Fig. 2 – Sketch of an oxide ion conducting solid oxide fuel cell showing the different species conduction to and from the triple phase boundaries at the electrodes. Graphic design by Adrián Robles-Férnandez.

or YSZ-Mullite [61–63]. In contrast with composites produced by traditional ceramic methods, the solidified eutectics have much less proportion of grain boundaries, so that their contribution to resistivity will be smaller. Moreover, the directionality of the microstructure will contribute to optimize the connectivity of the conducting phase. On the contrary, the constraints of the eutectic composition with limited phase content of conducting phase and the limitations to modulate its doping content work against reaching conductivity values comparable to the best single phase electrolyte ceramics. As a result, the highest conductivity at 1000 K among the above composites is the one of YSZ (with 9 mol% Y_2O_3)-Al_2O_3, 2×10^{-3} S/cm [64], close to one order of magnitude smaller than that of 8YSZ (ZrO_2 with 8 mol% Y_2O_3). Attempts to minimize the shortcomings have been made by solidifying off-eutectic compositions richer in the conducting phase [65] or by doping [62]. Primary dendrites of the excess phase form, with severe modification of the resultant composite microstructure. Increase in conductivity over the eutectic by a factor of 2.6 has been achieved in ZrO_2 rich 3YZ(3 mol% Y_2O_3 doped ZrO_2)-Al_2O_3 composites solidified by LFZ under specific conditions. In other eutectics such as YSZ-$BaZrO_3$ and CaSZ (Calcia stabilized ZrO_2)-NiO both component phases are electrical conductors. Adjacent to ion conducting stabilized zirconia, NiO shows electronic hole conduction and doped $BaZrO_3$ either hole or proton conduction, depending on the equilibrium atmosphere and temperature. Unfortunately the amount of Y doping in $BaZrO_3$ phase that could be achieved by LFZ processing was limited [66]. The influence of a large hetero-interface density in a rather aligned microstructure was also studied on ZrO_2 containing eutectics, as large interface densities result naturally at solidification at high pulling rates. Samples with ZrO_2 (3 mol% Y_2O_3) platelet thickness down to 70 nm were prepared, which encompassed a cell microstructure. No evidence of interface enhanced or depressed conductivity was observed [65].

Composite materials combining both ion and electron conducting phases are the basis of many applications such as, for example, electrodes in different electrochemical devices (fuel cells, electrolysers, gas sensors, membranes, etc.). In the case of solid oxide fuel cells (SOFC) or electrolysers (SOEC), besides the percolation of both electrical species, the presence of a network of interconnected pores is necessary in order to allow the flow of gas (oxygen or fuel depending on the type of electrode: cathode or anode) to the so-called triple phase boundaries (TPB) where the reactions take place (Fig. 2). In order to obtain a high number of these active TPB, the nature and stability of the microstructure of the material is crucial [67]. Different strategies have been explored in the literature in order to increase the number of TPB by reducing the average particle size of at least one of the phases [68,69]. However, high operation temperatures above 700 °C often lead to microstructural evolution processes limiting long-term stability. In the case of the most commonly used SOFC anodes containing Ni particles in combination with YSZ or gadolinium-doped ceria (GDC), the cell degradation is mainly dictated by the sintering of said nickel particles and the associated decrease of TPB [70]. Since Ni particles provide the catalytic properties to the electrode, the decrease of its active surface will be detrimental for the overall performance. Besides, undesired oxidation of Ni particles to NiO (or $Ni(OH)_2$ in operation under high steam concentration) and their subsequent expansion may result in irreversible and fatal cracks in the electrode.

Lamellar electrodes produced by reduction of textured YSZ-based eutectics obtained from the melt have been proposed as an alternative to the traditional fuel electrodes [71] (Fig. 3). The eutectic CaSZ-NiO or CaSZ-$Ni_{1-x}Co_xO$ had been solidified using an optical image furnace by Dhalenne and Revcolevschi [72,73]. It consists of around 30 vol% of CaSZ and NiO or $Ni_{1-x}Co_xO$ solid solution [71]. We have obtained eutectic microstructures consisting of alternating YSZ and NiO (CoO) oxide lamellae with interlamellar spacing around 1 μm by LFZ methods. Subsequent reduction of the eutectic materials in 5%H_2/Ar atmosphere at temperatures above 600 °C allows the transformation of NiO (CoO) to Ni (Co), yielding a ~42% porous metallic phase where the pore network improves the fuel flow to the TPB. The metallic phase acts as the electron conducting path in the electrode, with

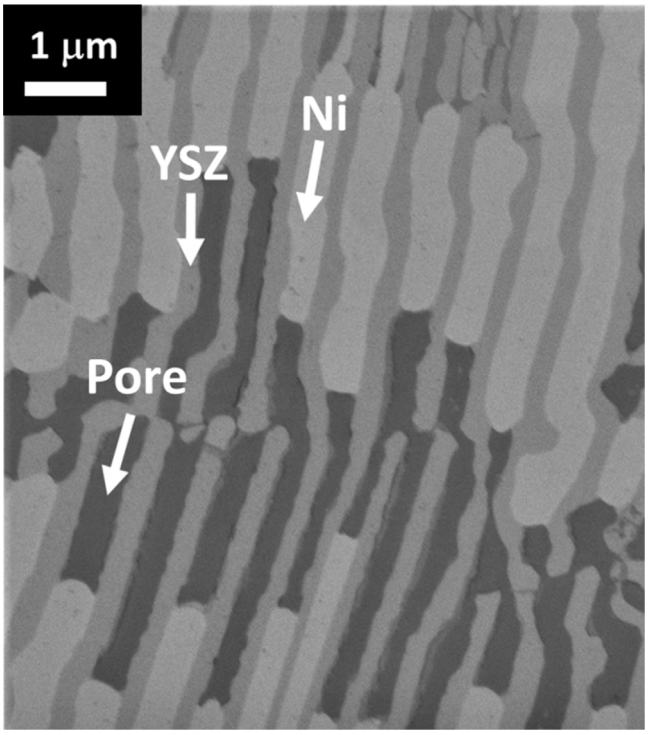

Fig. 3 – SEM image of a YSZ-NiO eutectic ceramic grown at 100 mm/h, after reduction at 600 °C for 10 h under 5%H_2. The bright phase is Ni, the grey one corresponds to YSZ, and the darkest one is porosity.

lower ohmic resistances than equivalent isotropic composites. Meanwhile, the diffusion of the oxide ions takes place preferentially along the YSZ phase with activation energies somewhat larger than those for pure YSZ, owing to the doping with the transition metal. The so prepared textured electrodes present various advantages such as their high temperature microstructural stability, since Ni particles grain growth is hindered due to the low-energy interfaces formed between the metallic Ni or Co particles and the YSZ lamellae [74–76].

Aiming to enhance the electro-catalytic activity of the anodes through the extension of the reaction sites beyond the surface of the metallic phase, equivalent lamellar eutectic materials have been developed based on CeO_2 and GDC instead of YSZ [77,78]. An advantage of such electrodes is that they could be used in combination with GDC electrolytes, allowing lower operation temperatures than their YSZ counterparts. This decrease in operation temperature has always been targeted in order to increase the stability and durability of these SOEC devices [79]. While stabilized ZrO_2—NiO gave rise always to a lamellar eutectic microstructure, at all pulling rates, in CoO—CeO_2 a microstructural cross-over under specific solidification conditions was observed [80]. The microstructure was rod-like at low puling rates (10 mm/h), associated to a change in the overall solidified composition that took place during solidification. Selective evaporation and migration into the melt (segregation) are pointed out as responsible for this behaviour. Both, evaporation and migration can be enhanced by relatively large thermal gradients in the melt and the large free-surface-to-volume ratio of the melt in the solidification by LFZ.

Since eutectic materials have a high density of interfaces, whose nature appears relevant to their performance, a thorough study of the crystallographic orientation relationships and interfaces was made in this family. The most common orientation relationship found for the mentioned NiO—YSZ, NiO—CeO_2, NiO—GDC, CoO—YSZ, CoO—CeO_2 and CoO—GDC eutectics is given by (1 1 1)TMO//(0 0 1)IC,TMO being the transition metal oxide and IC the ionic conductor. Eutectic growth is ruled by minimization of the interfacial energy, therefore, this interface corresponds to the best match between ionic charges and the maximum overlapping of reciprocal lattices of both phases forming the interphase [81,82]. Upon reduction to form TM/IC cermets, different orientation relationships have been observed [83], with either topotactic transformation from the TMO to the TM, or reorientation to create epitaxial interfaces of the metal with the exposed surfaces of the IC. In all cases it appears that these newly created surfaces are very stable. In the specific case of materials for SOEC, it is also important to study the possible segregation effects of dopants towards these interfaces and their effects on the functional properties. Recently it has been shown how the relaxation of the lattice and charge mismatch is achieved through segregation of the dopant to the interphase (Gd in the GDC-CoO system) [84]. Kelvin probe force microscopy experiments point towards enhanced interfacial ionic conductivity probably due to the higher disorder of the interfacial oxygen plane.

High temperature membranes

Mixed conduction, either present in the same compound or owned by a composite material consisting of appropriate complementary phases, can afford membrane applications for selective gas permeation. In a recent research an innovative application of eutectics has been proposed. The natural ordering of these systems is exploited to produce a porous matrix that, after infiltration with molten carbonates and under a difference in CO_2 partial pressure as driving force, allows the CO_2 transport. Carbonate anions migrate through the liquid with compensating oxide ions migrating through the ion conducting solid oxide. The porous material is obtained from the eutectic bycrystal of Mg stabilized zirconia—MgO by selective dissolution of the minority phase. ZrO_2—MgO eutectics are known to form coupled fibrous like microstructures, as predicted by the minimum of interface energy criteria, since its solidification by the Bridgman method in molybdenum crucibles [85,86]. The component phases are highly refractory, with melting points around 2700 °C and 2800 °C, while the eutectic temperature is around 2100 °C, and the solidification at atmospheric pressure is straightforward. Coupled fibrilar microstructure can be achieved by LFZ at pulling rates below 25 mm/h [87]. Fibre (MgO) dissolution results in a porous ion conducting matrix with highly dense, well aligned parallel pores of very uniform diameter, all aspects facilitating permeation. Infiltrating this porous structure with a ternary eutectic mixture of Li, Na and K carbonates as molten salt, a high CO_2 permeability of 1.41×10^{-10} mol m^{-1} s^{-1} Pa^{-1} has been obtained at 815 °C [88]. These are permeability values similar to the ones observed in membranes based on other better conducting ceramics produced by more conventional

ceramic preparative methods. The specific microstructure that results from the directional solidification appears to be essential to achieve the high permeation.

High temperature ceramics for thermophotovoltaic emitters

Another property of thermomechanically resistant oxide eutectics that has been studied is their performance as selective thermal emitters for applications in thermophotovoltaic devices. Thermophotovoltaic generators rely on a hot radiator, emitting in the near infrared, to pump a photovoltaic cell to generate electricity [89–91]. The heat would come either from waste heat of from other available sources. The task of the appropriate thermal emitter is to avoid emission at wavelengths longer than the ones that can be used by the photocell, as well as very energetic ones, so as not to waste the available energy. This excess energy would heat the system above optimum operating temperatures. Rare earth oxides or transition metal doped oxide thick coatings or felts were initially tested [92–95]. When the directionally solidified oxides demonstrated excellent mechanical properties, eutectics that contained rare earth oxides as components or others doped with transition metal ions were proposed for this application. The laser floating zone method here provides again suitable samples for testing, but also for the eventual fabrication of the emitter coupled to a device, as the thin rod shape will support rather fast heating and cooling cycles to which it might be submitted upon use. Added to that, the same configuration (namely heating of a small sample volume by laser irradiation) was used by P.B. Oliete and colleagues to measure the selective emission without contamination from radiation from other sources, as the nearby materials were much cooler (at room temperature). Selective thermal emission has been measured in Al_2O_3—RE_2O_3 (RE = rare earth) [96,97], Al_2O_3—RE_2O_3—ZrO_2 [98], MgO—MgSZ:TM (TM = transition metal) [87] or MgO—$MgAl_2O_4$:TM (in preparation). Several interesting results were found: rare earth containing eutectics show much more selective emission than transition metal ion doped ones, matching the sharp RE^{3+} absorption bands which show small broadening and shifting with temperature; the selectivity is sharper for RE concentrations far below 100% in the eutectic; ZrO_2 in the Al_2O_3—RE_2O_3—ZrO_2 or MgO—ZrO_2 eutectics introduces a broad emission band which makes the composite a worse candidate when compared with a eutectic without the defective ZrO_2 phase; and the selectivity of TM doped eutectics degrades strongly for very moderate TM ion concentrations.

Selective laser melting

In the preceding section we have reported on a number of materials that were solidified by the LFZ method. Eutectics with coupled growth at relatively fast solidification rates (small-sized microstructure) require the LFZ technique to be solidified. In other examples, the solidified material reacts with the surrounding atmosphere (selective evaporation or change in oxygen content) so that the phase distribution across the solidified samples might be specific for the procedure. Therefore, the knowledge gained by the solidification of these materials by LFZ is very helpful to find conditions for other procedures that involve melting. In selective laser melting a small volume of the material is molten (the melt pool), adjacent to an unmelted substrate or supporting stage and travels along the piece to generate a new layer or region of the material, solidified, adhered to the substrate. The procedure can proceed by melting new layers on the material already processed (with new powder addition), or be used to melt selectively specific areas of the surface for sealing or texturing (surface laser melting), polishing (decrease roughness), welding, marking (involving melting) or coating. Lasers are well suited for these selective melting procedures as they are widely available and are easier to incorporate in industry than other radiations. They can also be focused into small volumes, down to 30 μm with near infrared lasers [99] allowing processing resolution. As such, selective laser melting is one specific technique of additive manufacturing (AM) [100], which is well established in the processing of polymers or metals, but not yet for ceramic processing. Many reviews can be found in the literature [101–104], updating the state-of-the art of additive manufacturing by selective laser processing at each moment, since its invention in the late 1980s. Today, it is a very active field in industrial development, deployment and research activity, based on the potentialities to achieve final processed parts in one (or very few) steps, customized and with low raw material and energy consumption. Moreover, it can afford the processing of complex shaped pieces not possible by other procedures. The overall procedure of selective laser sintering/melting encompasses a computer controlled laser beam that deposits localized energy at precise locations and rates on a plane, and a procedure to add new material to the processing area. Techniques differ mainly in the way to add new material to the previous layer, and the process that takes place in the matter as a consequence of its interaction with the laser beam. The directed radiation (the laser beam) can heat to promote sintering (with or without partial melting, as in selective laser sintering, SLS), directly melt the material (as in selective laser melting, SLM, directed energy deposition, DED, or laser engineering net shaping, LENS) or generate consolidation by other processes such as polymerization of a photoresin (as in stereolithography).

Surface laser melting of an already consolidated object is easier than additive manufacturing by laser melting since there is no need to renew the material to process and the balling risk of added loose powder particles is eliminated. However, both involve melting and solidification processes and fast temperature variations. The surface laser melting of ceramics, in essence equivalent to Zone Melting, is sketched in Fig. 4. The material to treat is located on the processing stage in the processing area, where the laser beam is scanned. Preheating the sample is often needed, and this can be done by locating the processing area inside a furnace [105] (with access windows for the processing laser, visualization and thermal cameras), a hot plate [106] or heating by another means [107,108]. Protective gases are fed to the processing area. CO_2 ($\lambda = 10.6$ μm) or NIR lasers (high power diode, Nd:YAG o Nd:YVO_3 at $\lambda = 1.07$ μm) are commonly used, either CW or pulsed with long pulse duration. The laser beam will scan the sample surface describing an established pattern at a defined scan rate and hatch space (distance between consecutive lines). A melt pool will be formed, which will travel on the sample surface with the laser beam, generating a resolidified

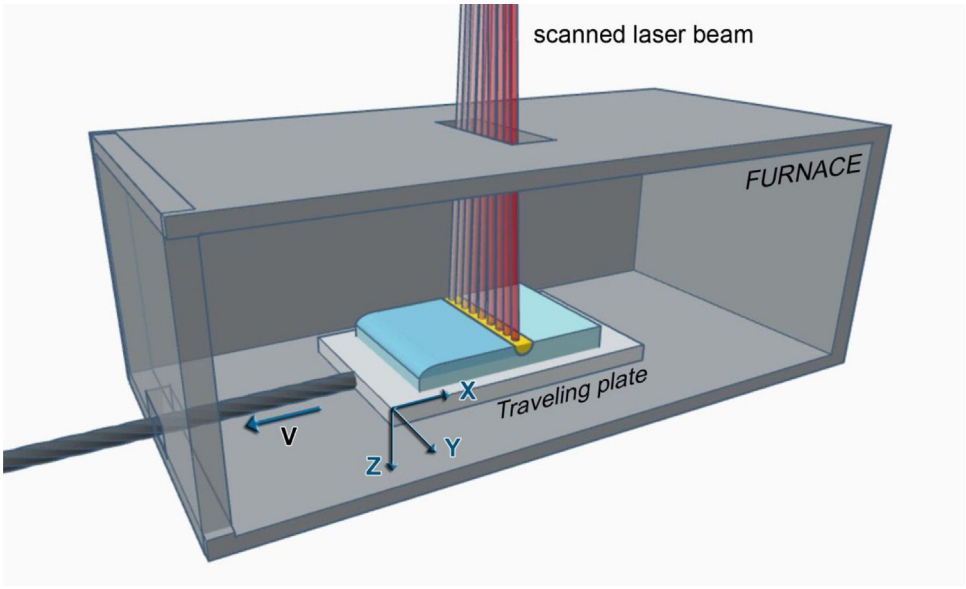

Fig. 4 – Sketch of the surface laser melting procedure as used presently at our laboratory. In the example the laser energy is scanned on the sample, equivalently to a line of uniform intensity along the Y direction, and travels at a predefined traverse speed along the X direction. The concept is similar to other surface laser melting equipment, as referred to in the text.

layer. In the case of a linearly scanned laser beam (as in the figure along the Y direction) the movement in the other direction (X) can also be provided by an independent translation table. The laser-line can be shaped with optical means, promoted by laser construction (e.g. linear diode stacks) or be an effective one produced by scanning a static line repetitively on the surface with the rate appropriate to the thermal properties of the material to be processed. In this case, the solidification direction will be contained in the XZ plane all along the processing, and the solidification rate will be determined by the traverse speed of the translation table.

To process white ceramics (such as Al_2O_3 or ZrO_2), which are poor absorbers of the NIR radiation at RT, absorption enhancing additives have been sometimes added. Ester et al. added Mn or Co oxides to Al_2O_3 based eutectic ceramics [109], and L. Ferrage et al. mixed carbonaceous slurries with the ceramic oxide [110]. The parameters that define the processing are laser power, beam size, laser scan rate (exposure time and point distance) and hatch space or table traverse velocity when it is the case [99]. The optimum scanning rate is a compromise of productivity, control of microcracking and desired microstructure (texture and phase size). Fast solidification rates of eutectic composites, as the ones used by H. Huang [111] and D. Wu [112] in LENS of ZrO_2—Y_2O_3—Al_2O_3 composites produce colony microstructrures with submicrometer interspacings, and the repetitive layering causes a banded microstructure.

The brittleness of ceramics has been one main drawback to develop AM or surface treatment procedures with direct melting, and the need to add non-localized heat to prevent cracks was recognized and tested. Wilkes and colleagues [113,114] designed and patented an apparatus that added a homogenized defocused CO_2 laser beam that heated the processing area up to 1600 °C, and included also preheating of the powder reservoir. Moreover, they processed a eutectic mixture of ZrO_2 and Al_2O_3 which is tougher than either Al_2O_3 or zirconia. This allowed them to consolidate complex shapes of Al_2O_3—ZrO_2 ceramics by additive manufacturing SLS/M. Previously, researchers of surface laser melting processes in ceramics had also added preheating in a furnace [115], proven that eutectic Al_2O_3—ZrO_2 ceramics were suitable composites for laser surface melting [116], and tested other ways of preheating different ceramics. F.H. Stott and colleagues combined a flame or another laser to assist the laser processing [107,108]. Others used specifically built furnaces to preheat the ceramics [105]. In particular, for ZrO_2(3molY_2O_3)—Al_2O_3 $40 \times 40\,mm^3$ surface areas were successfully resolidified free from cracks at travelling rates of 1000 mm/h and with 1200 °C preheating in a continuous furnace [117].

In Fig. 5 we give the temperature profile measured by thermal imaging at 632 nm the surface-melting (steady state) of a piece of ZrO_2 (3 mol%Y_2O_3)—Al_2O_3 eutectic. Sintered pellets preheated at 980 °C were processed with a line-shaped high power diode laser ($\lambda = 922$ nm) [118]. From these measurements, the thermal gradient before and behind the melt pool are determined. The gradient at the solidifying solid–liquid interface diminishes as the solidification rate increases because traverse speed and thermal transport towards the cooler parts of the material compete. It ranged from 3×10^5 K/m at a traverse speed of 2880 mm/h to an extrapolated value of 7.5×10^5 K/mm at very low traverse speeds [119]. These are solidification gradients similar to the ones measured in LFZ solidification. From these values, the heating and cooling rates are determined for the different traverse speeds. As seen in the figure, the cooling rate tends to saturate as the traverse speed increases.

Most of the research on selective laser melting of ceramics for AM has been done with ceramic biomaterials or structural materials. There are very few works in the literature devoted to selective laser sintering/melting applied to materials for energy. Zirconia is an exception given its broad range of

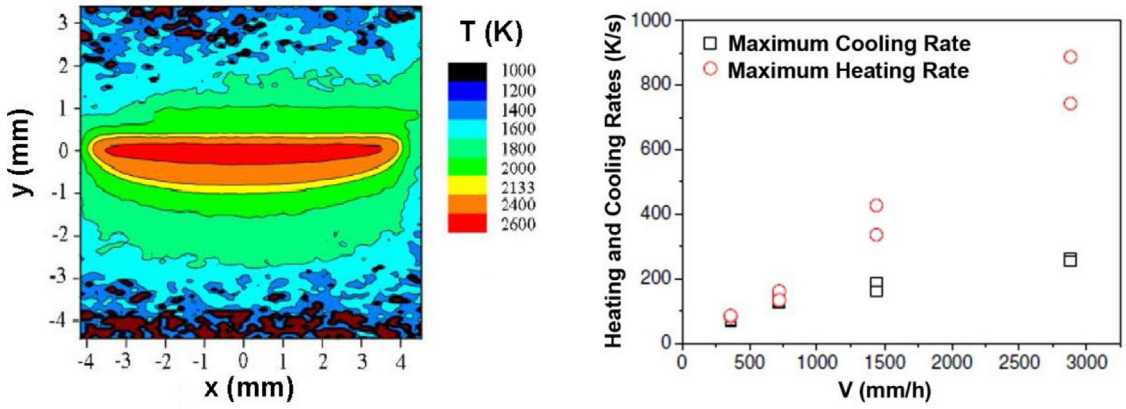

Fig. 5 – Left: temperature map of a ZrO_2 (3 mol%Y_2O_3)-Al_2O_3 eutectic plate (7.5 mm wide) at processing with a laser line, 1 mm wide, linear power P = 105 W/cm, traverse speed = 1440 mm/h, preheating = 980 °C, which gives a 510 μm depth remelted layer. Positive Y values are pristine non melted areas, negative Y values are processed areas. The contour line between yellow (the brighter band in gray scale) and orange corresponds to the melting temperature of the material. Right: Maximum heating and cooling rates of the solid at the surface at different traverse speeds, adapted from [118].

applications, also as bioceramic or structural ceramic. In the field of conventional lithium batteries with liquid electrolyte, selective laser sintering techniques have been used to obtain cathodes with 3D structures with increased power density. Manufacturing electrodes with high energy and power densities simultaneously is challenging as their requirements are in competition. To increase the energy density, it is necessary to resort to thick electrodes that increase the mass per unit volume. In contrast, high volumetric power densities require large surface area electrodes to allow high speed capability. The 3D structuring of the electrode offers a balance between both requirements. Thus, SLS has been used with nickel cobalt and aluminium oxide cathodes $LiNi_{0.80}Co_{0.15}Al_{0.05}O_2$ in which the laser beam selectively consolidates regions of a powder bed of the material layer by layer until the three-dimensional structure is built [120]. Laser technology has also been used to carry out electrode crystallization, especially in micro-battery architectures with thin cathodes. Conventional anneals at high temperatures and long times restrict the choice of materials for current collectors and substrates, in addition to causing the loss of lithium in the cathode material. The use of lasers then allows one to carry out processes where the high temperature is restricted to local areas and short times. This technique has been used to carry out, among others, surface anneals of $LiMn_2O_4$ cathodes to control cubic spinel crystallization, a process that is very sensitive to both synthesis temperatures and the Li/Mn ratio [121]. Regarding the new generation of solid–state batteries, recent studies explore the ability of laser technology to sinter ionic conductors that act as electrolytes [122].

Selective laser processing for SOCs

There have been several trials to process zirconia by selective laser processing, and difficulties have been encountered in selective laser sintering or melting procedures. Ferrage [123] reports consolidated parts with simple geometry with up to 96% density, consisting of textured material. Verga [124] shows complex shaped parts made out of alumina toughened zirconia with mm size features and moderate fracture strengths. These methods seem promising to manufacture scaffolds and structured patterns, useful for example to support SOC structures or electrodes. For fully dense, thin layers of YSZ, successful results have been obtained by stereolithography. For example, Pesce et al. [125] used a commercial ceramic 3D printer equipped with a UV semiconductor laser (around 0.5 W) to selectively cure a ceramic loaded slurry that contained photocurable resin. The layering step was 25 μm, a good enough resolution to print high aspect ratio corrugated YSZ electrolyte, with the associated decrease in ASR of the SOFC cells. The process, though, requires long post-processing steps to eliminate the organic content and sinter without defects. Ruiz-Morales et al. [126] review the AM procedures used for the manufacture of SOC devices. Up to date the most successful trials to get dense YSZ layers have been stereolithography or ink-jet printing on cermet substrates.

Composites withstand better the large thermal stresses inherent to selective laser melting. As NiO-stabilized ZrO_2 composites with the eutectic composition are appropriate for fuel electrodes in SOFCs or other catalytic processes, they have been processed by surface laser melting and explored as electrodes in those cells. NIR or FIR wavelength lasers are equally well suited to the processing of this material, as NiO absorbs effectively enough the NIR radiation. As observed for the Al_2O_3 based eutectics [116,127], the thick (several 100 μm) solidified layer possesses a graded microstructural size and alignment, following the shape of the solid–liquid boundary (melt pool), with finer interspacing at the external surface (see Fig. 6). These features respond to the thermal transport (heating and dissipation) processes, which include absorption of the laser light at the outermost layer hit by the laser beam, heat transport in the melt aided by convection currents and heat dissipation by radiation and thermal conduction towards the solid substrate. At low traverse speeds, also the composition of the resolidified layer is graded [128], as a result of composi-

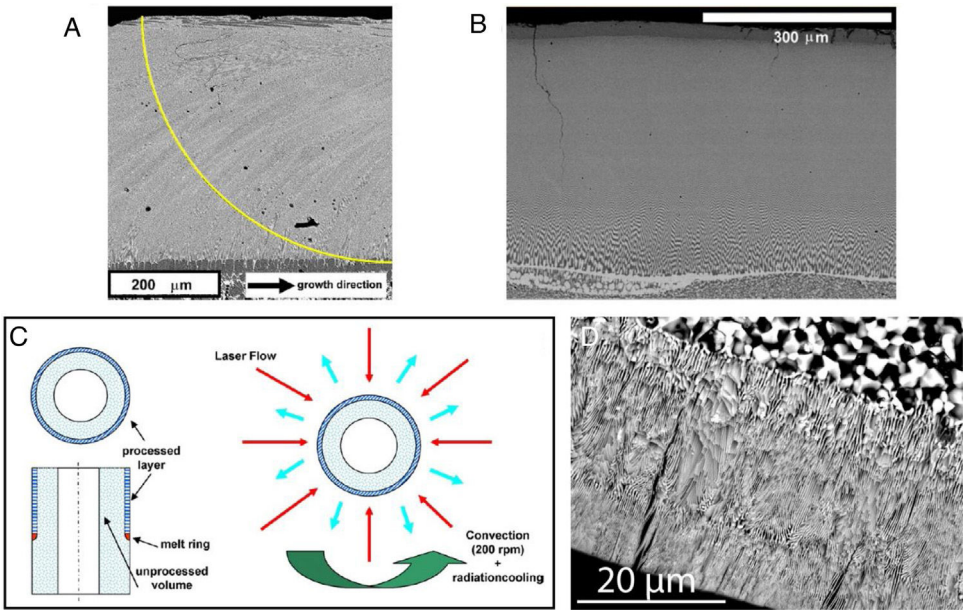

Fig. 6 – (a) SEM image of a cross section in the longitudinal direction of a CaSZ-NiO laser surface melted piece. The superposed line indicates the approximate shape of the solid–liquid interface (solidification front), which determines the alignment of the microstructure [127]; (b) SEM image of a cross section in the transverse direction of a hypo-eutectic YSZ-NiO composite processed with traverse speed of 60 mm/h [128]; (c) diagram showing the surface laser melting procedure used to generate the layer shown in d [130]; (d) (transverse cross section) of a laser-processed tube, after thermochemical reduction and acid etching to remove metallic Ni.

tion gradients and the convection currents built-in in the melt. These surface laser processed plates have been coated with dense YSZ layers produced by vapour phase deposition [129] and then thermochemically reduced. The result is a porous cermet (Ni-YSZ)/dense-YSZ arrangement that mimics anode supported SOFCs. Surface laser melting has also been applied to porous NiO-YSZ microtubes [130]. The procedure is shown in Fig. 6. These authors achieved a 25 μm thick remelted layer on the outer surface of the microtubes with lamellar interphase spacing around 200 nm and radial alignment. Under the fast solidification and rotation conditions imposed, the cooling of the melt appeared to be dominated by radiation and convection. A further attempt to take advantage of this solidified eutectic in SOFC was made by Cubero et al. [131]. They prepared YSZ pellets coated with a NiO-YSZ slurry, which were then surface laser melted with traverse speeds between 1 and 10 m/s. They could achieve 20 μm thick cermet layers with fine eutectic microstructure. Tested as SOFCs, they measured lower (around 1/2) polarization resistance than with sintered coatings. It is difficult to control the melt depth, as this small volume is determined by a balance between larger magnitudes, the laser heating power and the dissipation processes (radiation, convection and conduction). Careful control of the process parameters is required.

In spite of the better performance of the textured cermets and although there are ways to get this texture on differently shaped substrates, these approaches have not been incorporated yet into the SOFC manufacture routines. It would require the optimization of several other steps in the manufacture of the finished device.

Selective laser melting of other composite ceramics

The thermal shock resistance requirement of suitable selective emitters for thermophovoltaics that prompted the study of emissive properties of solidified eutectics in the systems Al_2O_3—RE_2O_3 (RE = rare earth), makes them suitable for the additive manufacture processes based on selective laser melting, in the same way as it was recently done with Al_2O_3—YAG or Al_2O_3—YAG—YSZ composites by Z. Fan [132,111]. Oliete et al. [133] surface melted a previously dip-coated and sintered Al_2O_3—$ME_3Al_5O_{12}$ (ME = Er or Yb) coating on a 3 mm diameter Al_2O_3 rod (see Fig. 7b), with a similar set-up as the one employed to texture the tubes described in the previous paragraph, and studied its thermal emission. No preheating was used in this case. The coating was around 125 μm thick once remelted and was well adhered to the Al_2O_3 rod (Fig. 7c and d). The surfaces of Al_2O_3—$Er_3Al_5O_{12}$ composite pellets have also been laser melted at different traverse speeds, with and without eutectic compositions, in the frame of an investigation of the emissivity vs. microstructure and layer thickness (Fig. 7a). As the toughness of these composites (Al_2O_3—$ME_3Al_5O_{12}$) is smaller than the one of Al_2O_3—$ZrO_2(Y_2O_3)$ composites, a higher preheating temperature had to be used, 1300 °C, for up to 2 cm wide crack-free coated plate.

High preheating temperatures are also required to use surface laser melting with MgSZ—MgO eutectic mixtures. Using 1350 °C (preheating temperature), a CO_2 laser beam scanned with a linear power density = 76 W/cm and traverse speeds of 50–150 mm/h, layers around 0.5 mm thick have been solidified on 10 mm × 20 mm × 2 mm previously sintered plates. Fig. 8 shows a piece of the plate. The microstructure of the treated area is given in the micrograph (same Fig. 8). Apart from slight

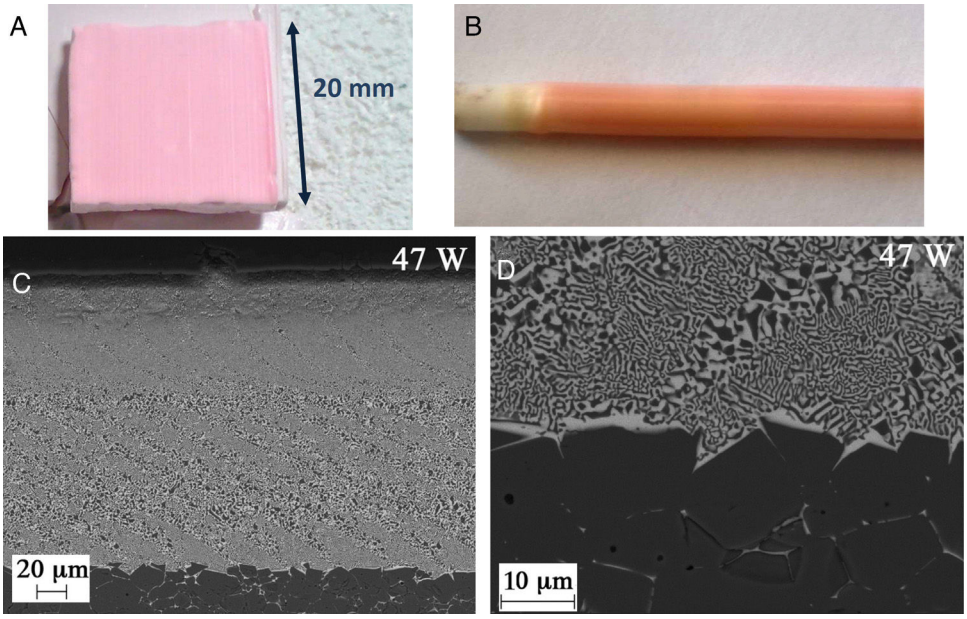

Fig. 7 – Al_2O_3—$Er_3Al_5O_{12}$ surface laser melted samples. (a) plate; (b) coating on 3 mm diameter Al_2O_3 dense ceramic rod; (c) SEM micrograph of coating shown on b; (d) detail of the coating-Al_2O_3 interface. (c) and (d) from Oliete et al. [132,133].

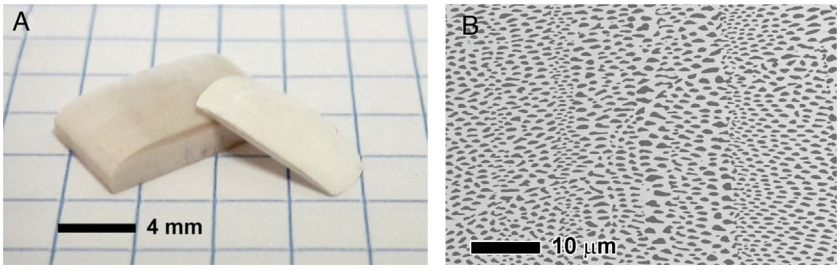

Fig. 8 – Left: Piece of ZrO_2—MgO pellet with the laser melted surface (thick sample), with rounded edges. The brownish tinge is an optical effect of the sample microstructure. The thinner slice is the cut and polished solidified layer after acid etching. Right: SEM micrograph of one MgO—ZrO_2 surface melted eutectic sample after polishing the upper surface. The bright phase is MgSZ, the darker one is MgO. Note that the image shown corresponds to a plane parallel to the larger plate surface, at a distance (some tens of microns) from the upper surface.

banding, it is consistent with the MgO-fibre in MgSZ matrix microstructure that forms in directionally solidified samples. After acid etching to eliminate MgO, using the same procedure as in [88], the weight loss suggests that all the MgO was eliminated, an indication that also in this case the MgO phase is connected to the outer surface of the material, and so will be the porosity after etching. Laser surface melting allows producing several cm^2 of porous YSZ plate material with around 30 vol% pore size in the micron range. Submicron size porosity was also found by Campana et al. [130] on acid treated Ni-YSZ tube cermets with the surface textured by laser melting. Further studies on the pore distribution and performance of these structures as CO_2 membranes are under way.

Laser machining and structuring

Traditional surface machining of ceramics includes techniques such as grinding or polishing. However, using these techniques, ceramics are extremely difficult to machine into complex shapes with high accuracy and efficiency due to their hardness and brittleness. On the contrary, laser ablation is nowadays a convenient alternative. A laser beam is highly directional, coherent and monochromatic, delivering extremely high energy in a small area (down to the order of $\sim 1\,\mu m^3$ with appropriate focusing), that may produce locally very high temperatures (>20,000 K) [134,135]. Pulsed lasers deliver tremendous amounts of light power densities in a very short interaction time (down to femtoseconds). In addition, as the interaction area is very small, the high rates of heating and cooling, practically not possible to attain by conventional techniques, can achieve higher material removal rates in almost any type of engineering material.

In fact, the use of lasers for machining different advanced structural ceramics (mainly Al_2O_3 or ZrO_2) has been demonstrated using various types of laser (Nd:YAG, CO_2, and excimer) in both continuous or pulse mode [136,137]. For the efficient machining of structural ceramics, pulse modes are in general

preferred as higher temperatures are achieved, typically above the vaporization temperature, resulting in higher material removal rates mainly by evaporation but also by melt expulsion and dissociation. In any case, achieving higher material removal along with a desired surface finish is a critical issue to be studied and optimized in each case. Key parameters are wavelength, power density and pulse duration of laser beam and optical, thermal and mechanical properties of the material to be machined. Diffraction bounds the size of the laser beam to several microns wide. Overall, diffraction, thermal diffusivity and beam dispersion limit practical laser processing spatial resolution to more than 25 μm even for the shortest laser wavelength available. Nevertheless, direct laser interference patterning (DLIP) has been used to produce micron size periodic patterns on polymers and ceramics [138], as for example on hydroxyapatite materials. In this procedure, the laser provides a fundamental wavelength of 1064 nm (Nd:YAG). An applied wavelength of 355 nm (or 266 nm) was obtained by third (or fourth) harmonic generation and the laser beam was then split into two coherent laser beams, which interfered on the substrate surface. The interference process produces micropatterns with periodical distances of about 10 μm [139]. This is at present the finest machining available in direct laser processing. Generally speaking, these processes include laser drilling, laser cutting, and laser grooving, marking or scribing.

Laser machining of ceramics is recently attracting great interest in energy related technologies that generate or convert energy more efficiently, such as solar cells, fuel cells, electrolysers, batteries or membranes. All these applications face similar challenges – higher efficiencies, lower costs, increased energy density and greater durability. This technology is being used widely for developing advanced solar cells. For example, cells with efficiencies as high as 21.4% have been fabricated by laser ablation. A Nd:YVO_4 laser was used to locally ablate a rear surface SiO_2 thermal passivation layer over the boron- and phosphorus-diffused regions before applying the inter-digitized finger metallization in an Emitter Wrap Through (EWT) solar cell [140]. In addition, lasers have also been used to drill arrays of small holes through wafers in the fabrication of Metal Wrap Through (MWT) and EWT back contact solar cells.

Laser drilling

The laser drilling technique has been efficiently used in metals and polymers [141,142], and in recent years has been largely implemented for drilling ceramics. Several examples can be found in electrochemical energy devices. Holes were successfully produced using ultrashort laser pulses of 20 mJ and 40 fs (femtoseconds) in a Fe—22Cr mesh dipped into $LaNi_{0.6}Co_{0.4}O_{3-\delta}$ (LNC), $LaNi_{0.6}Fe_{0.4}O_{3-\delta}$ (LNF) and $(La_{0.8}Sr_{0.2})_{0.95}Fe_{0.6}Mn_{0.3}Co_{0.1}O_3$ (LSFMC) slurries to form alternative contact composites for SOFC, without influencing the system performance [143]. Different laser systems were used for drilling holes and also for sintering AFC (alkaline fuel cell) components, mainly metals and polymers [144]. Membrane patterning using pulsed laser micromachining was also proposed for enhancing PEMFC performance. An increase in performance by a factor of 3.6 was demonstrated with very low catalyst loadings [145]. A Nd-YAG laser (pulse width in the nanosecond range) was also used for drilling holes with 20–32 μm effective diameters in brass sheets leading to porous supports with 1.6 and 18% porosity. The inherent properties of brass as a metal support together with its chemical compatibility with ZIF-8 (an imidazolate-based metal–organic framework compound) and its activation by the laser treatment (generation of roughness and ZnO from Zn oxidation) promoted the nucleation and crystal growth of different micro-membranes, producing a high quality, continuous membrane with gas transport through the micropores [146]. Laser texturing has proven to be a very useful tool to increase the performance of lithium ion batteries (LIBs), for example by modifying (perforating, etc.) the current collectors [147] or the selective ablation of the composite materials used as electrodes [148]. One of the main causes of decrease in the battery potential with respect to the theoretical one are the diffusion overpotentials in the electrodes soaked in liquid electrolyte due to the limited diffusion of Li in materials with low porosity and high tortuosity, which generates concentration gradients of the lithium salt in the liquid. These gradients are even more pronounced in high-power batteries with high electric currents. This is where appropriate structuring of the electrodes comes into play, having obtained very promising results both in the cathode compounds and in the graphite normally used as anode in said batteries [149]. Regarding anode materials in LIBs, SnO_2 has interesting electrochemical properties that are shadowed by the enormous volume changes that occur during cycling, causing microstructural instabilities and loss of capacity. In this case, laser ablation makes it possible to create structure patterns in the electrode that allow compensation for said volume expansion [150]. Also within anode materials, microchannel perforations improve the response of electrodes based on 2D materials such as graphene [151]. All these examples show the efficiency of laser drilling for different materials. However, its implementation for drilling ceramics with high accuracy and efficiency still has challenges.

In recent years, we have successfully implemented this technology to drill Ni-YSZ cermets, the state of the art SOFC anode material. Ni-YSZ anodes were machined to produce micron-size channels to improve gas permeation, thus reducing concentration polarization of SOFCs. Usually, advanced ceramics are commonly machined once sintered, which results in low efficient machining processes due to both the high hardness and brittleness of the ceramic samples [152]. In addition, depending on the features of the laser beam, heat transfer to surrounding areas takes place during the laser-ceramic interaction, resulting in a heat affected zone, HAZ, resolidified material on the surface and even the formation of microcracks. These shortcomings are usually tackled by decreasing the pulse duration to the pico- or femtosecond regime or by machining with laser wavelengths in the UV spectral range [2]. Nevertheless, a novel and highly efficient approach was found by machining the ceramic anode compacts before sintering [153,154]. Whilst laser ablation mechanisms in the sintered ceramic were due to both optical and thermal processes, in the green compact, an additional mechanical ablation mechanism was also involved. The pulsed laser radiation at 1064 nm in the nanosecond range was

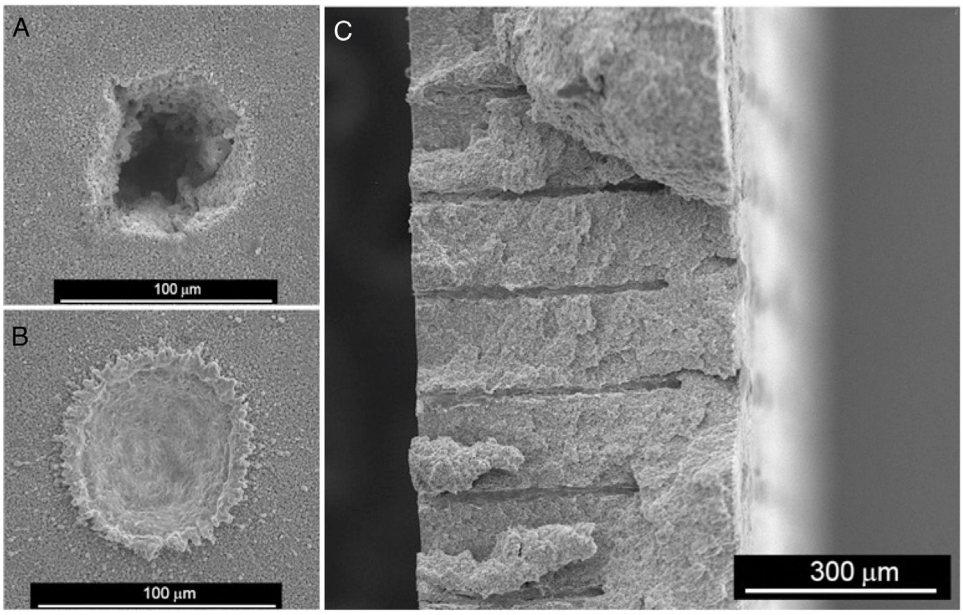

Fig. 9 – Micrographs of drillings performed in the NiO-YSZ compact substrate (a), and reduced Ni-YSZ cermet substrate (b) [153]. Cross-section micrograph of a general view of the drills performed in a 450 μm thick NiO-YSZ compact before sintering (c) [154].

absorbed by the organic material present in the compact, pyrolyzing it and giving rise to a gas jet which dragged the surrounding material. In addition, the material was removed without significant heating of the adjacent areas, leading to a cold ablation mechanism. As an example, Fig. 9(a) and (b) shows the resulting drilled holes respectively in the compact and in the cermet (sintered and thermochemically reduced material). In addition to the higher efficiency achieved by machining the compact before sintering, other adverse effects are avoided, such as the great amount of redeposited metallic debris inside the drilled hole and in the surroundings of the processed areas when drilling the cermet.

The drilling performance rate was found to be more than 16 times larger in the unsintered compact than in the sintered ceramic [153,154]. Further optimization of the drilling process showed that the most suitable YSZ/NiO ratio was 30/70 in vol% and that the highest yield, around 90,000 μm^3 per pulse, was found at a laser irradiance of 6.9 GW/cm^2. Furthermore, the diameter of the drilled hole remained essentially constant at around 10 μm, as shown in Fig. 9(c), in a 450 μm-thick NiO-YSZ anode substrate.

Laser drilling produces precise drilled holes in ceramics as well as single crystals. For this reason, the procedure was chosen to prepare perforated ceramic specimens to study the fundamentals of CO_2 permeation of oxide–molten carbonate membranes [155]. Perforated pores in single crystals have allowed to optically monitor the gas–liquid interface and to extract CO_2 permeation rates at very low driving forces. The technique was also used to fabricate a leak-free tubular-supported molten-salt membrane with 1000 parallel laser-drilled pores that made possible the measurement of CO_2 permeation rates without issues related to the sealing procedure.

Laser machining

In addition to concentration polarization reduction, pulse laser machining has been also used to reduce the ohmic losses in SOFCs [156]. For this application, yttria-stabilized zirconia (YSZ) is the most used electrolyte in Solid Oxide Fuel Cells because of its remarkable mechanical properties, chemical stability, and developed synthesis and manufacture technology. Furthermore, electrolyte-supported SOFCs are preferred in terms of robustness and resistance to thermal and redox cycles of the cell [157]. Taking into account that the ideal situation would be the fabrication of electrolytes thinner than 20–50 μm, but still presenting good mechanical properties, a novel laser-assisted method to produce self-supported thin ionic conducing membranes was developed [156,158]. For example, honeycomb patterns were machined in 150 μm-thick YSZ plates by using a pulsed laser source with emission at 532 nm and pulse duration in the nanosecond range. Laser machining parameters were optimized to achieve removal rates of 0.2 mm^3/s and 1785 μm^3 per pulse, typical values for this type of sintered advanced ceramics [159,160]. Fig. 10 shows the micrograph of the fracture cross-section view of the machined plate (a) and a detail of the bottom (b).

Impedance spectroscopy characterization showed that the Area Specific Resistance (ASR) of the laser-machined plates was decreased by a factor of 2.8 compared to the non-machined electrolyte. The performance of the laser-machined electrolytes was also tested by preparing a single cell using Ni-YSZ and LSM-YSZ as electrodes. It was observed that the ASR_{cell} of the machined sample was smaller than for the case of the blank sample. Moreover, the cell power densities at 750 °C and 0.7 V increased by a factor of more than 50% [156]. Finally, it was confirmed that a thin layer of 8YSZ

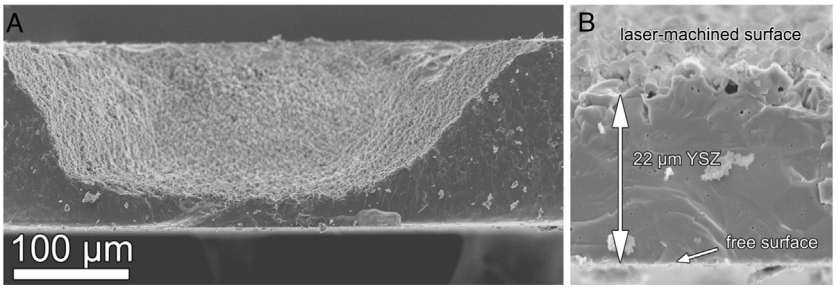

Fig. 10 – Micrograph of the fracture cross-section view of the machined YSZ plate (a) and a detail of the bottom (b).

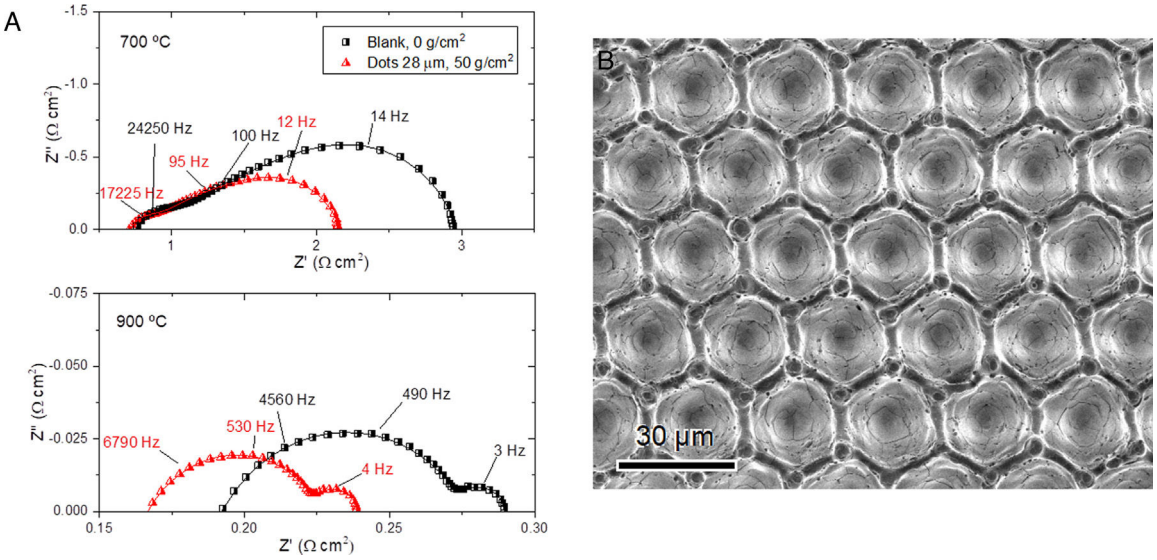

Fig. 11 – (a) EIS analysis of the unprocessed and patterned symmetrical cells after engraving a square lattice ($a = 28\ \mu m$, depth ~7 µm) at 700 °C (top) and 900 °C (bottom). (b) SEM plan-view image of the YSZ surface of a laser-machined hexagonal arrangement ($a = 24\ \mu m$, depth ~22 µm).

nanoparticles coats the processed surface, and that this layer is not detrimental to the electrochemical performance of the membranes. On the contrary, EIS experiments showed that the polarization resistance of LSM/YSZ cathodes deposited on the membranes actually decreases by about 5%, in comparison with unprocessed YSZ samples [158].

Laser structuring

Once the value of the electrolytic ohmic impedance has been reduced, mostly using thin film electrolytes in electrode-supported configurations, the main contribution to cell losses is the activation polarization of the cathode, as the anode kinetics for H_2 oxidation is much faster than cathode kinetics for O_2 reduction [161]. One of the main concepts to reduce the activation polarization is to increase the electrode–electrolyte contact surface in order to enhance the reaction rate by means of a larger Triple Phase Boundary (TPB) length [162]. The first suggestion in this direction was probably introduced by Herbstritt et al., depositing by screen-printing large YSZ (YSZ: $Zr_{1-x}Y_xO_{2-\delta}$) particles onto the electrolyte surface [163]. Afterwards, other strategies have been proposed, such as to impregnate the cathode with nanoparticles near the interface [164,165] or to develop different types of templates at the nanoscale with significant electrode–electrolyte area enlargement [166,167]. Nevertheless, nanotechnology-based strategies usually present durability concerns associated to coarsening of nano-assemblies and the high operation temperature [168,169]. Methods based on ceramic technology, as the first one proposed by Herbstritt et al., seem more appropriate for large-scale applications. For instance, atmospheric plasma spraying [170], imprinted micro-patterns [171] and, more recently, microextrusion printing [172] have been proposed to increase the surface roughness of the electrolyte.

In recent years, we have addressed an innovative approach to enlarge the electrode–electrolyte contact area incorporating a new laser-machining step to the cell fabrication, but basically maintaining the most successful ceramic components and methods already tested in SOFC. We engrave a periodic pattern in the mesoscale range (10–100 µm) onto the electrolyte or electrode surface by laser ablation. The pattern design is defined through a Computer Assisted Design (CAD) file that controls the laser beam, usually in the green wavelength region ($\lambda = 532$ nm) and with a pulse width of 5 ns. Laser machining or structuring does not involve a significant extra

cost in the cell fabrication. In addition, laser machining is able to produce repeatable periodic microstructures that are very convenient for comparing the experimental results with model calculations obtained under periodic boundary conditions.

In the first tests carried out based on this approach, as a proof of concept [173], we engraved onto a sintered YSZ electrolyte a micro-pattern consisting in a square lattice of ~7 μm deep wells and lattice parameter $a = 28\,\mu m$. To obtain good electrode–electrolyte contact after sintering and avoid debinding in the bottom of the well, it was necessary to assist the sintering with low loads of about 5 kPa. The low load used did not modify the electrode microstructure. The electrochemical characterization of laser surface modified LSM-YSZ/YSZ/LSM-YSZ (LSM: $La_{1-x}Sr_xMnO_3$) symmetrical cells demonstrated that the polarization resistance decreased by about 30% with respect to the unprocessed surfaces, which roughly matched the electrode–electrolyte contact area enlargement calculated from optical profilometry. In addition, EIS analysis confirmed that the polarization reduction obtained could be ascribed to activation processes (Fig. 11a).

In a second and more ambitious test, we succeeded in preparing surfaces with a hexagonal arrangement of ~22 μm deep wells and lattice parameters $a = 24\,\mu m$ (Fig. 11b), resulting in surface enlargement factors about 2.4 [174]. However, this radical geometry, accessible with this technology, presents two main drawbacks. On the one hand, the thickness of the active region, where the electrochemical reactions take place, is about 10–15 μm [175], which is of the same order of magnitude as the depth and lattice parameter of the patterned surfaces. As a consequence, the real increase in exchange current density would be related to the increase in the active volume region adjacent to the electrolyte, but not to the increase in geometrical contact surface. Therefore, it was determined that the increase in exchange current density for the above-mentioned surface should be ~40–80%, which is still a significant figure. On the other hand, we have verified that the conventional ceramic suspensions commonly used for cathode deposition onto flat surfaces are not suitable for highly corrugated surfaces. Therefore, new ceramic formulations with increasing solids loadings and appropriate viscosity were prepared. The best results were obtained using an ethanol-based formulation with 20 wt% solids loading and a viscosity of 21 mPa s at a shear rate of $10\,s^{-1}$. Under these conditions we obtained a reduction by ~50% of the activation component of the polarization resistance, which matches pretty well with the increase in the interfacial active volume. However, the gas diffusion component increased significantly due to excessive cathode densification. Appropriate electrode gas diffusion was restored using a suspension formulation with lower solids loading and higher viscosity, but the activation component decrease obtained in this manner is lower than expected, probably because of the excessive cathode porosity inside the wells [174]. Therefore, we are currently working in machining shallower wells and using optimized ceramic suspensions for depositing the cathode on this kind of surfaces [176]. As a result, laser machining has been confirmed as a powerful and versatile tool for modifying the microstructure of the electrode–electrolyte contact surface, improving the electrochemical cell performance.

Conclusions

Lasers in the processing of ceramic materials are used in many different procedures. Some are already at the industrial level, others still under research or development. From the review of these technologies as used to process ceramic oxides for two particular energy applications: electrochemical cells and selective emitters for thermophotovoltaics, one can conclude the following.

LFZ can be used to grow from the melt some of the oxide materials providing samples for research of their fundamental properties. It is particularly well suited for the solidification of high temperature melting oxide eutectics with a broad range of interface spacing and homogeneous (coupled) microstructure. LFZ experiments also provide knowledge about the feasibility and conditions for melt processing.

Selective laser sintering/melting has not yet been explored to process oxides for SOFCs or batteries. The technique is still focused in other fields of ceramic processing such as composite oxide ceramics and bioceramics, at the research level. The much simpler related process of surface laser melting has been explored with eutectic composite materials with functional properties and microstructural characteristics adequate to high temperature electrochemical devices (SOFCs or molten carbonate membranes). Successful plates and coatings of a few cm^2 size were demonstrated and their functional performance could already be tested in some cases. The procedure can now be judged as scalable. Composite oxides with excellent mechanical properties such as Al_2O_3 based eutectics, or particularly the selective emitters Al_2O_3—$ME_3Al_5O_{12}$ (ME = rare earth oxide) have also been successfully applied as coatings by surface laser melting on plates or tubes. Advances on laser melting additive manufacturing techniques of these composites are also being made.

The subtractive processing of materials with laser (drilling, machining or structuring) has also proven applicability in the field. Efficient hole drilling was demonstrated for Ni-YSZ cermet fuel-electrode materials. Machining and structuring of the YSZ electrolyte impact positively in the performance of SOFC and SOEC devices. The incorporation of some of these processes in the manufacture has to compete with very advanced device ceramic processing procedures that tend to be more cost effective in large scale manufacture. However, significant increase in performance or durability of the device will be the motivation to develop the whole manufacturing process incorporating laser processing.

Acknowledgments

The authors thank Prof. Víctor M. Orera, to whose memory this work is dedicated, for his continuous encouragement and support in carrying out this research. We also acknowledge the financial support from the Spanish Ministerio de Ciencia e Innovación through grants PID2019-107106RB-C32/AEI/10.13039/501100011033 and RTI2018-098944-J-I00 (MCIU/AEI/FEDER, UE) and from the Departamento de Ciencia, Universidad y Sociedad del Conocimiento del Gobierno de Aragón through the financial support to the Research

Group T02_20R. Authors would like to acknowledge also the Servicio General de Apoyo a la Investigación SAI, Universidad de Zaragoza, namely, the Service of Electron Microscopy of Materials.

REFERENCES

[1] M. William, Steen Laser Material Processing, 3rd ed., Springer Verlag, Berlin, 2003.
[2] D. Bäuerle, Laser Processing and Chemistry, 4th ed., Springer Verlag, Berlin, 2011.
[3] N. Schiavon, V. Melfos, R. Salzer, et al., Applying the techniques on materials, in: A.E. Varella (Ed.), Conservation Science for the Cultural Heritage. Lecture Notes in Chemistry 79, Springer Verlag, 2013, pp. 247–332, http://dx.doi.org/10.1007/978-3-642-30985-4_6, ISBN 978-3-642-30985.
[4] P. Baglioni, D. Chelazzi, R. Giorgi, G. Poggi, Colloid and materials science for the conservation of cultural heritage: cleaning, consolidation, and deacidification, Langmuir 29 (2013) 5110–5122, http://dx.doi.org/10.1021/la304456n.
[5] L. Luvidi, A.M. Mecchi, M. Ferretti, G. Sidoti, Treatments with self-cleaning products for the maintenance and conservation of stone surfaces, Int. J. Conserv. Sci. 7 (2016) 311–322.
[6] E. Di Francia, R. Lahoz, D. Neff, V. Rico, N. Nuns, E. Angelini, S. Grassini, Novel procedure for studying laser-surface material interactions during scanning laser ablation cleaning processes on Cu-based alloys, Appl. Surf. Sci. 544 (2021) 148820, http://dx.doi.org/10.1016/j.apsusc.2020.148820.
[7] R. Lahoz, Ablación láser de materiales inorgánicos y metálicos (PhD Thesis), 2006.
[8] F. Rey-García, R. Ibáñez, L.A. Angurel, F.M. Costa, G.F. de la Fuente, Laser Floating zone growth: overview, singular materials, broad applications, and future perspectives, Crystals 11 (2021) 38, http://dx.doi.org/10.3390/cryst11010038.
[9] M.A. Laguna-Bercero, M.L. Sanjuán, R.I. Merino, Raman spectroscopic study of cation disorder in poly- and single crystals of the nickel aluminate spinel, J. Phys. Condens. Matter 19 (2007) 186217, http://dx.doi.org/10.1088/0953-8984/19/18/186217.
[10] V.M. Orera, C. Pecharromán, J.I. Peña, R.I. Merino, C.J. Serna, Vibrational spectroscopy of $CaZrO_3$ single crystals, J. Phys. Condens. Matter 10 (1998) 7501, http://dx.doi.org/10.1088/0953-8984/10/33/019.
[11] M. Bassat, P. Odier, A. Villesuzanne, C. Marin, M. Pouchard, Anisotropic ionic transport properties in La_2NiO_{4+d} single crystals, Solid State Ion. 167 (2004) 341–347, http://dx.doi.org/10.1016/J.SSI.200312012.
[12] V. Granata, R. Fittipaldi, A. Guarino, A. Ubaldini, E. Carleschi, A.M. Strydom, F. Chiarella, A. Vecchione, Crystal growth of the Ca_2RuO_4-Ru metal system by the floating-zone technique, J. Alloys Compd. 832 (2020) 154890, http://dx.doi.org/10.1016/j.jallcom.2020.154890.
[13] H.J. Scheel, T. Fukuda, Crystal Growth Technology, John Wiley & Sons Ltd., Chichester, UK, 2003.
[14] P. Rudolph, T. Fukuda, Fiber crystal growth from the melt, Cryst. Res. Technol. 34 (1999) 3–40.
[15] D. Sola, F.J. Ester, P.B. Oliete, J.I. Peña, Study of the stability of the molten zone and the stresses induced during the growth of Al_2O_3-$Y_3Al_5O_{12}$ eutectic composite by the laser floating zone technique, J. Eur. Ceram. Soc. 31 (2011) 1211–1218, http://dx.doi.org/10.1016/j.jeurceramsoc.2010.08.022.
[16] F.J. Ester, J.I. Peña, Análisis de la zona fundida en el crecimiento del compuesto eutéctico Al_2O_3–$ZrO_2(Y_2O_3)$ por fusion zonal con láser, Bol. Soc. Esp. Ceram. V 46 (2007) 240–246, http://dx.doi.org/10.3989/cyv.2007.v46.i5.225.
[17] J.L. Schmehr, M. Aling, E. Zoghlin, S.D. Wilson, High-pressure laser floating zone furnace, Rev. Sci. Instrum. 50 (2019) 043906, http://dx.doi.org/10.1063/1.5085327.
[18] S. Uda, T. Tsubota, Ionic impurity transport and partitioning at the solid–liquid interface during growth of lithium niobate under an external electric field by electric current injection, J. Cryst. Growth 312 (2010) 3650–3657, http://dx.doi.org/10.1016/j.jcrysgro.2010.09.052.
[19] P. Rudolph, Travelling magnetic fields applied to bulk crystal growth from the melt: the step from basic research to industrial scale, J. Cryst. Growth 310 (2008) 1298–1306, http://dx.doi.org/10.1016/j.crysgro.2007.11.036.
[20] R.S. Feigelson, Pulling optical fibers, J. Cryst. Growth 79 (1986) 669–680, http://dx.doi.org/10.1016/0022-0248(86)90535-X.
[21] J.K.R. Weber, J.J. Felten, B. Cho, P.C. Nordine, Glass fibres of pure and erbium- or neodymium-doped yttria–alumina compositions, Nature 393 (1998) 769–771, http://dx.doi.org/10.1038/31662.
[22] N. Soleimani, B. Ponting, E. Gebremichael, A. Ribuot, G. Maxwell, Coilable single crystal fibers of doped-YAG for high power laser applications, J. Cryst. Growth 393 (2014) 18–22, http://dx.doi.org/10.1016/j.jcrysgro.2013.11.036.
[23] J. Llorca, V.M. Orera, Directionally solidified eutectic ceramic oxides, Prog. Mater. Sci. 51 (2006) 711–809, http://dx.doi.org/10.1016/j.pmatsci.2005.10.002.
[24] F.J. Ester, D. Sola, J.I. Peña, Efectos Térmicos Inducidos durante el crecimiento del compuesto eutéctico Al_2O_3–$ZrO_2(Y_2O_3)$ por fusion zonal con láser, Bol. Soc. Esp. Ceram. V 47 (2008) 7–12, https://boletines.secv.es/upload/199837256.pdf.
[25] S. Kou, Transport Phenomena in Materials Processing, John Wiley and Sons Inc., New York, 1996.
[26] G.F. de la Fuente, J.C. Diez, L.A. Angurel, J.I. Peña, A. Sotelo, R. Navarro, Wavelength dependance in laser floating zone processing. A case study with Bi–Sr–Ca–Cu–O superconductors, Adv. Mater. 7 (1995) 853, http://dx.doi.org/10.1002/adma.19950071008.
[27] M.A. Borik, S.I. Bredikhin, V.T. Bublik, A.V. Kulebyakin, I.E. Kuritsyna, E.E. Lomonova, P.O. Milovich, V.A. Myzina, V.V. Osiko, P.A. Ryabochkina, N.Y. Tabachkova, Structure and conductivity of yttria and scandia-doped zirconia crystals grown by skull melting, J. Am. Ceram. Soc. 100 (2017) 5536–5547, http://dx.doi.org/10.1111/jace.15074.
[28] D.A. Agarkov, M.A. Borik, S.I. Bredikhin, I.N. Burmistrov, G.M. Eliseeva, V.A. Kolotygin, A.V. Kulebyakin, I.E. Kuritsyna, E.E. Lomonova, F.O. Milovich, V.A. Myzina, P.A.N. Ryabochkina, Yu. Tabachkova, T.V. Volkova, Structure and transport properties of zirconia crystals co-doped by scandia, ceria and yttria, J. Materiomics 5 (2019) 273e279, http://dx.doi.org/10.1016/j.jmat.2019.02.004.
[29] J. Martínez-Fernández, A.R. Pinto-Gómez, J.J. Quispe-Cancapa, A.R. de Arellano-López, J. Llorca, J.Y. Pastor, S. Farmer, A. Sayir, High-temperature plastic deformation of Er_2O_3-doped ZrO_2 single crystals, Acta Mater. 54 (2006) 2195–2204, http://dx.doi.org/10.1016/j.actamat.2006.01.012.
[30] A. Ridruejo, J.Y. Pastor, J. LLorca, A. Sayir, V.M. Orera, Stress corrosion cracking of single-crystal tetragonal $ZrO_2(Er_2O_3)$, J. Am. Ceram. Soc. 88 (11) (2005) 3125–3130, http://dx.doi.org/10.1111/j.1551-2916.2005.00573.x.
[31] M.R.N. Soares, C. Nico, M. Peres, N. Ferreira, A.J.S. Fernandes, T. Monteiro, F.M. Costa, Structural and optical properties of europium doped zirconia single crystal fibers

grown by laser floating zone, J. Appl. Phys. 109 (2011) 013516, http://dx.doi.org/10.1063/1.3527914.
[32] K. Kasaki, J. Maier, Re-analysis of defect equilibria and transport parameters in Y_2O_3-stabilized ZrO_2 using EPR and optical relaxation, Solid State Ion. 134 (2000) 303–321, http://dx.doi.org/10.1016/S0167-2738(00)00766-9.
[33] M.A. Laguna-Bercero, V.M. Orera, Micro-spectroscopic study of the degradation of scandia and ceria stabilizaed zirconia electrolytes in solid oxide electrolysis cells, Int. J. Hydrogen Energy 36 (2011) 13051–13058, http://dx.doi.org/10.1016/j.ijhydene.2011.07.082.
[34] A. Robles, A. Orera, J.I. Peña, R.I. Merino, in preparation.
[35] F.W. Dynys, M.H. Berger, A. Sayir, Laser processed protonic ceramics, J. Eur. Ceram. Soc. 28 (2008) 2433–2440, http://dx.doi.org/10.1016/j.jeurceramsoc.2008.03.038.
[36] M.J. López-Robledo, C. Vaquero-Aguilar, J. Martínez-Fernández, J.I. Peña, A. Sayir, M. Jiménez-Melendo, Processing and mechanical behavior at elevated temperatures of directionally solidified proton conducting perovskites, J. Eur. Ceram. Soc. 31 (2011) 1339–1344, http://dx.doi.org/10.1016/j.jeurceramsoc.2010.05.0224.
[37] J. Ramírez-Rico, M.J. López-Robledo, A.R. de Arellano-López, J. Martínez-Fernández, A. Sayir, Fabrication and microstructure of directionally solidified $SrCe_{1-x}Y_xO_{3-\delta}$ ($x = 0.1$, 0.2) high temperature proton conductors, J. Eur. Ceram. Soc. 26 (2006) 3705–3710, http://dx.doi.org/10.1016/j.jeurceramsoc.2005.12.003.
[38] A. Várez, M.L. Sanjuán, M.A. Laguna, J.I. Peña, J. Sanz, G.F. de la Fuente, Microstructural development of the $La_{0.5}Li_{0.5}TiO_3$ lithium ion conductor processed by the laser floating zone (LFZ) method, J. Mater. Chem. 11 (2001) 125–130, http://dx.doi.org/10.1039/b003305g.
[39] Y. Maruyama, S. Minamimure, C. Kobayashi, M. Nagao, S. Watauchi, I. Tanaka, Crystal growth of $La_{2/3-x}Li_{3x}TiO_3$ by the TSFZ method, R. Soc. Open Sci. 5 (2018) 181445, http://dx.doi.org/10.1098/rsos.181445.
[40] P.B. Oliete, A. Orera, M.L. Sanjuán, Spectroscopic insight into the interplay between structural disorder and oxidation degree in melt-grown $Ce_{0.5}Zr_{0.5}O_{2-y}$ compounds, J. Raman Spectr. 51 (2020) 514–527, http://dx.doi.org/10.1002/jrs.5797.
[41] L. Grima, J.I. Peña and M. L. Sanjuán, to be published.
[42] V.S. Stubican, R.C. Bradt, Eutectic solidification in ceramic systems, Ann. Rev. Mater. Sci. 11 (1981) 267–297, http://dx.doi.org/10.1146/annurev.ms.11.080181.001411.
[43] V.M. Orera, J.I. Peña, Directional solidification, in: N.P. Bansal, A.R. Bocaccini (Eds.), Ceramics and Composites Processing Methods, The American Ceramic Society Publishing. John Wiley and Sons Inc., 2012.
[44] M. Parlier, R. Valle, L. Perrière, S. Lartigue-Korinek, L. Mazerolles, Potential of directionally solidified eutectic ceramics for high temperature applications, ONERA J. Aerospace Lab (2011) 1–13.
[45] R.I. Merino, J.I. Peña, A. Larrea, G.F. de la Fuente, V.M. Orera, Melt grown composite ceramics obtained by directional solidification: structural and functional applications, Recent Res. Devel. Mat. Sci. 4 (2003) 1–24.
[46] D.A. Pawlak, Eutectic fibers with self-organized structures, in shaped crystals: growth by micro-pulling-down technique, in: T. Fukuda, V.I. Chani (Eds.), Advances in Materials Research 8, Springer Verlag, Berlin, 2007, pp. 129–139.
[47] I. Saenko, O. Fabrichnaya, Thermodynamic database development for the ZrO_2–MgO–MnO_x system, J. Phase Equilib. Diffus. 41 (2020) 654–671, http://dx.doi.org/10.1007/s11669-020-00832-2.
[48] T. Ivas, E. Povoden-Karadeniz, N. Grundy, E. Jud-Sierra, J. Grässlin, L.J. Gauckler, Experimental phase diagram determination and thermodynamic assessment of the CeO_2-Gd_2O_3-CoO system, J. Am. Ceram. Soc. 96 (2) (2013) 613–626, http://dx.doi.org/10.1111/jace.12004.
[49] T. Goto, R. Tu, Eutectic ceramic composites by melt-solidification, J. Korean Ceram. Soc. 56 (2019) 331–339, http://dx.doi.org/10.4191/kcers.2019.56.4.02.
[50] F.S. Galasso, Unidirectionally solidified eutectics for optical, electronic and magnetic applications, J. Met. (1967) 17–21, http://dx.doi.org/10.1007/BF03378580.
[51] M. Diaz-Perez, L. Grima, B.M. Moshtaghioun, J.I. Peña, CaO–MgO–SiO_2–P_2O_5-based multiphase bio-ceramics fabricated by directional solidification: microstructure features and in vitro bioactivity studies, Ceram. Int. 47 (2021) 17041–17048, http://dx.doi.org/10.1016/j.ceramint.2021.03.011.
[52] M.F. Acosta, S.G. Rodrigo, L. Martín-Moreno, C. Pecharromán, R.I. Merino, Micropillar templates for dielectric filled metal arrays and flexible metamaterials, Adv. Opt. Mater. 5 (2017) 1600670, http://dx.doi.org/10.1002/adom.201600670.
[53] A. Kulkarni, E. Hanson, R. Zhang, K. Thornton, P.V. Braun, Archimedean lattices emerge in template-directed eutectic solidification, Nature 577 (2020) 355, http://dx.doi.org/10.1038/s41586-019-1893-9.
[54] D.A. Pawlak, S. Turczynski, M. Gajc, K. Kolodziejak, R. Diduszko, K. Rozniatowski, J. Smalc, I. Vendik, How far are we from making metamaterials by self-organization? The microstructure of highly anisotropic particles with an SRR-like geometry, Adv. Funct. Mater. 7 (2010) 1116–1124, http://dx.doi.org/10.1002/adfm.200901875.
[55] Y. Ohashi, N. Yasui, Y. Yokota, A. Yoshikawa, T. Den, Submicron-diameter phase-separated scintillator fibers for high-resolution X-ray imaging, Appl. Phys. Lett. 102 (2013) 051907, http://dx.doi.org/10.1063/1.4790295.
[56] A. Larrea, L. Contreras, R.I. Merino, J. Llorca, V.M. Orera, Microstructure and physical properties of CaF_2–MgO eutectics produced by the Bridgman method, J. Mater. Res. 15 (2000) 1314–1319, http://dx.doi.org/10.1557/JMR.2000.0190.
[57] B.M. Moshtaghioun, J.I. Peña, R.I. Merino, Medium infrared transparency of MgO–$MgAl_2O_4$ directionally solidified eutectics, J. Eur. Ceram. Soc. 40 (2020) 1703–1708, http://dx.doi.org/10.1016/j.jeurceramsoc.2019.10.053.
[58] K. Wysmulek, J. Sar, P. Osewski, K. Orlinski, K. Kolodziejak, A. Trenczek-Zajac, M. Radecka, D.A. Pawlak, A $SrTiO_3$–TiO_2 eutectic composite as a stable photoanode material for photoelectrochemical hydrogen production, Appl. Catal. B206 (2017) 538–546, http://dx.doi.org/10.1016/j.apcatb.2017.01.054, 0926-3373.
[59] Y. Liu, M. Zhang, Y. Nie, J. Zhang, J. Wang, Growth of YAG:Ce^{3+}–Al_2O_3 eutectic ceramic by HDS method and its application for white LEDs, J. Eur. Ceram. Soc. 37 (2017) 4931–4937, http://dx.doi.org/10.1016/j.jeurceramsoc.2017.06.014, 0955-2219.
[60] P.B. Oliete, A. Orera, M.L. Sanjuán, R.I. Merino, Selective thermal emission of directionally solidified $Al_2O_3/Y_{3-x}Er_xAl_5O_{12}$ eutectics: influence of the microstructure, temperature and erbium content, Sol. Energy Mater. Sol. Cells 174 (2018) 460–468, http://dx.doi.org/10.1016/j.solmat.2017.09.031.
[61] R.I. Merino, J.I. Peña, V.M. Orera, G.F. de la Fuente, Conductivity anisotropy in directionally solidified $CaZrO_3$–CaSZ and MgO–MgSZ eutectics, Solid State Ion. 100 (1997) 313–318, http://dx.doi.org/10.1016/S0167-2738(97)00347-0.
[62] R. Čička, V.M. Trnovcová, Y. Starostin, Electrical properties of alumina–zirconia eutectic composites, Solid State Ion.

148 (2002) 425–429, http://dx.doi.org/10.1016/S0167-2738(02)00082-6.
[63] R.G. Carvalho, A.V. Kovalevsky, M.W. Lufaso, R.F. Silva, F.M. Costa, F.M. Figueiredo, Ionic conductivity of directionally solidified zirconia–mullite eutectics, Solid State Ion. 256 (2014) 45–51, http://dx.doi.org/10.1016/j.ssi.2013.12.033.
[64] I. García, J.I. Peña, R.I. Merino, G.F. de la Fuente, V.M. Orera, Crecimiento de fibras ZrO_2 (Y_2O_3)–Al_2O_3 eutécticas mediante la técnica de fusión zonal inducida por láser, Bol. Soc. Esp. Ceram. Vidr. 37 (1998) 256–259, http://boletines.secv.es/upload/199837256.pdf.
[65] R.I. Merino, I. de Francisco, J.I. Peña, Ionic conductivity in directionally solidified Al_2O_3–ZrO_2(3 mol% Y_2O_3) near eutectic composites, Solid State Ion. 178 (2007) 239–247, http://dx.doi.org/10.1016/j.ssi.2006.12.017.
[66] R.G. Carvalho, A.J.S. Fernandes, R.F. Silva, F.M. Costa, F.M. Figueiredo, Directional solidification of ZrO_2–$BaZrO_3$ composites with mixed protonic–oxide ionic conductivity, Solid State Ion. 262 (2014) 654–658, http://dx.doi.org/10.1016/j.ssi.2013.10.051.
[67] S.D. Ebbesen, X. Sun, M.B. Mogensen, Understanding the processes governing performance and durability of solid oxide electrolysis cells, Faraday Discuss. 182 (2015) 393–422, http://dx.doi.org/10.1039/c5fd00032g.
[68] D.M. Amaya-Dueñas, G. Chen, A. Weidenkaff, N. Sata, F. Han, I. Biswas, R. Costa, K.A. Friedrich, A-site deficient chromite within situ Ni exsolution as a fuel electrode for solid oxide cells (SOCs), J. Mater. Chem. A 9 (9) (2021) 5685–5701, http://dx.doi.org/10.1039/d0ta07090d.
[69] Y. Lu, P. Gasper, U.B. Pal, S. Gopalan, S.N. Basu, Improving intermediate temperature performance of Ni-YSZ cermet anodes for solid oxide fuel cells by liquid infiltration of nickel nanoparticles, J. Power Sources 396 (2018) 257–264, http://dx.doi.org/10.1016/j.jpowsour.2018.06.027.
[70] A. Faes, A. Hessler-Wyser, D. Presvytes, C.G. Vayenas, J. VanHerle, Nickel–zirconia anode degradation and triple phase boundary quantification from microstructural analysis, Fuel Cells 9 (6) (2019) 841–851, http://dx.doi.org/10.1002/fuce.200800147.
[71] M.A. Laguna-Bercero, Á. Larrea, R.I. Merino, J.I. Peña, V.M. Orera, Stability of channeled Ni-YSZ cermets produced from self-assembled NiO-YSZ directionally solidified eutectics, J. Am. Ceram. Soc. 88 (11) (2005) 3215–3217, http://dx.doi.org/10.1111/j.1551-2916.2005.00540.x.
[72] G. Dhalenne, A. Revcolevschi, Directional solidification in the NiO–ZrO_2 system, J. Cryst. Growth 69 (1984) 616–618, http://dx.doi.org/10.1016/0022-0248(84)90374-9.
[73] L.N. Brewer, V.P. Dravid, G. Dhalenne, M. Velázquez, Solid-solution directionally solidified eutectic oxide composites: Part I. Eutectic growth and characterization, J. Mater. Res. 17 (2002) 760–767, http://dx.doi.org/10.1557/JMR.2002.0111.
[74] M.A. Laguna-Bercero, A. Larrea, R.I. Merino, J.I. Peña, V.M. Orera, Crystallography and thermal stability of textured Co-YSZ cermets from eutectic precursors, J. Eur. Ceram. Soc. 28 (12) (2008) 2325–2329, http://dx.doi.org/10.1016/j.jeurceramsoc.2008.01.019.
[75] M.A. Laguna-Bercero, A. Larrea, YSZ-induced crystallographic reorientation of Ni particles in Ni-YSZ cermets, J. Am. Ceram. Soc. 90 (2007) 2954–2960, http://dx.doi.org/10.1111/j.1551-2916.2007.01824.x.
[76] A. Larrea, M.A. Laguna-Bercero, J.I. Peña, R.I. Merino, V.M. Orera, Orientation relationship and interfaces in Ni and Co-YSZ cermets prepared from directionally solidified eutectics, Cent. Eur. J. Phys. 7 (2009) 242–250, http://dx.doi.org/10.2478/s11534-009-0030-z.
[77] L. Ortega-San-Martin, J.I. Peña, A. Larrea, V. Gil, V.M. Orera, Textured cermets of CeO_2 (or GDC) with Co for solid oxide fuel cells anodes, Int. J. Hydrog. Energy 35 (20) (2010) 11499–11504, http://dx.doi.org/10.1016/j.ijhydene.2010.05.013.
[78] L. Ortega-San-Martín, V. Gil, J.I. Peña, A. Larrea, V.M. Orera, Redox behaviour and ageing of GDC-Co cermets: a comparison between lamellar and conventional cermets, Solid State Ion. 226 (2012) 30–36, http://dx.doi.org/10.1016/j.ssi.2012.08.008.
[79] H. Yokokawa, H. Tu, B. Iwanschitz, A. Mai, Fundamental mechanisms limiting solid oxide fuel cell durability, J. Power Sources 182 (2) (2008) 400–412, http://dx.doi.org/10.1016/j.jpowsour.2008.02.016.
[80] L. Ortega-San-Martín, J.I. Peña, A. Larrea, V.M. Orera, Directionally solidified CeO_2 (or GDC)/CoO eutectic ceramics as cermet precursors for SOFCs anodes: microstructure cross-over, J. Eur. Ceram. Soc. 31 (2011) 1269–1276, http://dx.doi.org/10.1016/j.jeurceramsoc.2010.06.012.
[81] S. Serrano-Zabaleta, M.A. Laguna-Bercero, L. Ortega-San-Martín, A. Larrea, Orientation relationships and interfaces in directionally solidified eutectics for solid oxide fuel cell anodes, J. Eur. Ceram. Soc. 34 (9) (2014) 2123–2132, http://dx.doi.org/10.1016/j.jeurceramsoc.2013.06.008.
[82] S. Serrano-Zabaleta, A. Larrea, Calculation of the orientation relationships of directionally solidified eutectic ceramics by a modified coincidence of reciprocal lattice points model (CRLP), J. Am. Ceram. Soc. 99 (3) (2016) 1015–1022, http://dx.doi.org/10.1111/jace.13976.
[83] S. Serrano-Zabaleta, A. Larrea, A. Larrañaga, E.C. Dickey, Microstructure, texture, and crystallography in Ni-GDC and Co-GDC porous cermets obtained from directionally solidified eutectic ceramics, J. Mater. Sci. 52 (2017) 5477–5488, http://dx.doi.org/10.1007/s10853-016-0225-9.
[84] A. Orera, F. Wang, E. Ferreiro-Vila, S. Serrano-Zabaleta, A. Larrañaga, M.A. Laguna-Bercero, E.C. Dickey, F. Rivadulla, M.C. Muñoz, A. Larrea, Interfacial stability and ionic conductivity enhanced by dopant segregation in eutectic ceramics: the role of Gd segregation in doped CeO_2/CoO and CeO_2/NiO interfaces, J. Mater. Chem. A 8 (5) (2020) 2591–2601, http://dx.doi.org/10.1039/c9ta12315f.
[85] J. Echigoya, H. Suto, S. Hayashi, Growth morphology and orientation relationships in directionally solidified MgO–ZrO_2 eutectic, Trans. Jpn. Inst. Met. 26 (1985) 895–900, http://dx.doi.org/10.2320/matertrans1960.26.895.
[86] F.L. Kennard, R.C. Bradt, V.S. Stubican, Directional solidification of ZrO_2–MgO eutectic, J. Amer. Ceram. Soc. 57 (1974) 428–431, http://dx.doi.org/10.1111/j.1151-2916.1974.tb11374.x.
[87] D. Sola, P.B. Oliete, R.I. Merino, J.I. Peña, Directionally solidified Ni doped MgO-MgSZ eutectic composites for thermophotovoltaic devices, J. Eur. Ceram. Soc. 39 (2019) 1206–1213, http://dx.doi.org/10.1016/j.jeurceramsoc.2018.12.032.
[88] L. Grima, G.A. Mutch, P.B. Oliete, W. Bucheli, R.I. Merino, E.I. Papaioannou, J.J. Bailey, M.D. Kok, D.J.L. Brett, P.R. Shearing, I.S. Metcalfe, M.L. Sanjuán, High CO_2 permeability in supported molten-salt membranes with highly dense and aligned pores produced by directional solidification, J. Membr. Sci. 630 (2021) 119057, http://dx.doi.org/10.1016/j.memsci.2021.119057.
[89] T.J. Coutts, An overview of thermophotovoltaic generation of electricity, Sol. Energy Mater. Sol. Cells 66 (2001) 443–452, http://dx.doi.org/10.1016/S0927-0248(00)00206-3.
[90] B. Bitnar, W. Durisch, R. Holzner, Thermophotovoltaics on the move to applications, Appl. Energy 105 (2013) 430–438, http://dx.doi.org/10.1016/j.apenergy.2012.12.067.
[91] A. Datas, C. Algora, Development and experimental evaluation of a complete solar thermophotovoltaic system,

Prog. Photovolt: Res. Appl. 21 (2013) 1025–1039, http://dx.doi.org/10.1002/pip.2201.
[92] G.E. Guazzoni, High-temperature spectral emittance of oxides of erbium, samarium, neodymium and ytterbium, Appl. Spectrosc. 26 (1972) 60–65.
[93] D.L. Chubb, A.M.T. Pal, M.O. Patton, P.P. Jenkins, Rare earth doped high temperature ceramic selective emitters, J. Eur. Ceram. Soc. 19 (1999) 2551–2562, http://dx.doi.org/10.1016/S0955-2219(99)00096-5.
[94] B. Bitnar, W. Durisch, J.C. Mayor, H. Sigg, H.R. Tschudi, Characterisation of rare earth selective emitters for thermophotovoltaic applications, Sol. Energy Mater. Sol. Cells 73 (2002) 221–234, http://dx.doi.org/10.1016/S0927-0248(01)00127-1.
[95] L.G. Ferguson, F. Dogan, Spectral analysis of transition metal-doped MgO "matched emitters" for thermophotovoltaic energy conversion, J. Mat. Sci. 37 (2002) 1301–1308, http://dx.doi.org/10.1023/A:1014599924372.
[96] N. Nakagawa, H. Ohtsubo, Y. Waku, H. Yugami, Thermal emission properties of $Al_2O_3/Er_3Al_5O_{12}$ eutectic ceramics, J. Eur. Ceram. Soc. 25 (2005) 1285–1291, http://dx.doi.org/10.1016/j.jeurceramsoc.2005.01.031.
[97] P.B. Oliete, M.C. Mesa, R.I. Merino, V.M. Orera, Directionally solidified Al_2O_3–$Yb_3Al_5O_{12}$ eutectics for selective emitters, Sol. Energy Mater. Sol. Cells 144 (2016) 405–410, http://dx.doi.org/10.1016/j.solmat.2015.09.053.
[98] M.C. Mesa, P.B. Oliete, R.I. Merino, V.M. Orera, Optical absorption and selective termal emission in directionally solidified Al_2O_3–$Er_3Al_5O_{12}$ and Al_2O_3–$Er_3Al_5O_{12}$–ZrO_2 eutectics, J. Eur. Ceram. Soc. 33 (2013) 2587–2596, http://dx.doi.org/10.1016/j.jeurceramsoc.2013.05.001.
[99] E. Juste, F. Petit, V. Lardot, F. Cambier, Shaping of ceramic parts by selective laser melting of powder bed, J. Mater. Res. 29 (2014) 2086–2094, http://dx.doi.org/10.1557/jmr.2014.127.
[100] D. Grossin, A. Montón, P. Navarrete-Segado, E. Özmen, G. Urruth, F. Maury, D. Maury, C. Frances, M. Tourbin, P. l Lenormand, G. Bertrand, A review of additive manufacturing of ceramics by powder bed selective laser processing (sintering/melting): Calcium phosphate, silicon carbide, zirconia, alumina, and their composites, Open Ceramics 5 (2021) 100073, http://dx.doi.org/10.1016/j.oceram.2021.100073.
[101] D.L. Bourell, H.L. Marcus, J.W. Barlow, J.J. Beaman, Selective laser sintering of metals and ceramics, Int. J. Powder Metall. 28 (1992) 369–381, http://dx.doi.org/10.1016/0026-0657(93)90473-6.
[102] C.Y. Yap, C.K. Chua, Z.L. Dong, Z.H. Liu, D.Q. Zhang, L.E. Loh, S.L. Sing, Review of selective laser melting: materials and applications, Appl. Phys. Rev. 2 (2015) 041101, http://dx.doi.org/10.1063/1.4935926.
[103] J.J. Beaman, D.L. Bourell, C.C. Seepersad, D. Kovar, Additive manufacturing review: early past to current practice, J. Manuf. Sci. Eng. 142 (2020) 110812, http://dx.doi.org/10.1115/1.4048193.
[104] S. Pfeiffer, K. Florio, D. Puccio, M. Grasso, B.M. Colosimo, C.G. Aneziris, K. Wegener, T. Graule, Direct laser additive manufacturing of high performance oxide ceramics: A state-of-the-art review, J. Eur. Ceram. Soc. 41 (2021) 6087–6114, http://dx.doi.org/10.1016/j.jeurceramsoc.2021.05.035.
[105] L.C. Estepa and G. F. de la Fuente Leis. 2006. Continuous Furnace with Coupled Laser for the Surface Treatment of Materials, Patent number WO 2007/101900 A1.
[106] M. Mora, C. López-Gascón, L.A. Angurel, G.F. de la Fuente, The influence of support temperature on Bi-2212 monoliths textured by diode laser zone melting, Supercond. Sci. Technol. 17 (2004) 1329–1334, http://dx.doi.org/10.1088/0953-2048/17/11/015.
[107] L. Bradley, L. Li, F.H. Stott, Flame-assisted laser surface treatment of refractory materials for crack-free densification, Mat. Sci. Eng. A278 (2000) 204–212, http://dx.doi.org/10.1016/S0921-5093(99)00592-4.
[108] C. Triantafyllidis, L. Li, F.H. Stott, Surface treatment of alumina-based ceramics using combined laser sources, Appl. Surf. Sci. 186 (2002) 140–144, http://dx.doi.org/10.1016/S0169-4332(01)00639-0.
[109] F.J. Ester, R.I. Merino, J.Y. Pastor, A. Martín, J. LLorca, Surface modification of Al_2O_3–$ZrO_2(Y_2O_3)$ eutectic oxides by laser melting: processing and wear resistance, J. Am. Ceram. Soc 91 (2008) 3552–3559, http://dx.doi.org/10.1111/j.1551-2916.2008.02728.x.
[110] L. Ferrage, G. Bertrand, P. Lenormand, D. Grossin, B. Ben-Nissan, A review of the additive manufacturing (3DP) of bioceramics: alumina, zirconia (PSZ) and hydroxyapatite, J. Aust. Ceram. Soc. 53 (2017) 11–20, http://dx.doi.org/10.1007/s41779-016-0003-9.
[111] Z. Fan, Y. Zhao, Q. Tan, N. Mo, M.-X. Zhang, M. Lu, H. Huang, Nanostructured Al_2O_3-YAG-ZrO_2 ternary eutectic components prepared by laser engineered net shaping, Acta Mater. 170 (2019) 24–37, http://dx.doi.org/10.1016/j.actamat.2019.03.020.
[112] F. Niu, D. Wu, G. Ma, J. Wang, M. Gu, B. Zhang, Nanosized microstructure of Al_2O_3–ZrO_2 (Y_2O_3) eutectics fabricated by laser engineered net shaping, Scr. Mater. 95 (2015) 39–41, http://dx.doi.org/10.1016/j.scriptamat.2014.09.026.
[113] J.Y. Wilkes, C.H. Hagedorn, W. Meiners, K. Wissenbach, Additive manufacturing of ZrO_2–Al_2O_3 ceramic components by selective laser melting, Rapid Prototyp. J. 19/1 (2013) 51–57, http://dx.doi.org/10.1108/13552541311292736.
[114] S. Dierkes, A.J. Faber, J. Wilkes, M.P.M. Welters, W. Meiners, K. Wissenbach, Patent US 9,556 525 B2, 31 January 2017.
[115] S.Z. Lee, K.H. Zum Gahr, Surface treatments of Al_2O_3-ceramics by CO_2-lasers, Mat.-wiss. u. Werkstofftech 23 (1992) 117–123, http://dx.doi.org/10.1002/mawe.19920230406.
[116] A. Larrea, G.F. de la Fuente, R.I. Merino, V.M. Orera, ZrO_2–Al_2O_3 eutectic plates produced by laser zone melting, J. Eur. Ceram. Soc. 22 (2002) 191–198, http://dx.doi.org/10.1016/S0955-2219(01)00279-5.
[117] J. Gurauskis, V. Lennikov, G.F. de la Fuente, R.I. Merino, Laser-assisted, crack-free surface melting of large eutectic ceramic bodies, J. Eur. Ceram. Soc. 31 (2011) 1251, http://dx.doi.org/10.1016/j.jeurceramsoc.2010.08.017.
[118] F.J. Ester, Simulación y estudio experimental del método de solidificación superficial por láser aplicado a cerámicas eutécticas densas de sistema Al_2O_3–ZrO_2–Y_2O_3 (PhD Thesis), Universidad de Zaragoza, 2011.
[119] F.J. Ester, R.I. Merino, V.M. Orera, A. Martín, J.Y. Pastor, J. Llorca, Surface modification by laser melting of eutectic ceramic oxides, in: T.S. Sudarshan, M. Jeandin (Eds.), Surface Modification Technologies XXI (2008), 2008, pp. 297–304.
[120] K.A. Acord, A.D. Dupuy, U.S. Bertoli, B. Zheng, W.C. West, Q.N. Chen, A.A. Shapiro, J.M. Schoenung, Morphology, microstructure, and phase states in selective laser sintered lithium ion battery cathodes, J. Mater. Process. Technol. 288 (2021) 116827, http://dx.doi.org/10.1016/j.jmatprotec.2020.116827.
[121] X. Chen, J. Sastre, M. Rumpel, A. Flegler, A. Singhania, J. Balta Bonner, P. Hoffmann, Y.E. Romanyuk, Photonic methods for rapid crystallization of LiMn2O4 cathodes for solid-state thin-film batteries, J. Power Source 495 (2021) 229424, http://dx.doi.org/10.1016/j.jpowsour.2020.229424J.
[122] J.H.L. Silva, Y.G.S. Alves, A. Almeida, J.A. Moreira, R. Vilarinho, J.C.A. Santos, Y. Leyet, L.M. Jesus, R.S. Silva, Study of the ionic conductivity of $Li_{0.5}La_{0.5}TiO_3$ laser-sintered

ceramics, J. Eur. Ceram. Soc. 40 (2020) 5619–5625, http://dx.doi.org/10.1016/j.jeurceramsoc.2020.06.008.
[123] L. Ferrage, G. Bertrand, P. Lenormand, Dense yttria-stabilized zirconia obtained by direct selective laser sintering, Addit. Manuf. 21 (2018) 472–478, http://dx.doi.org/10.1016/j.addma.2018.02.005.
[124] F. Verga, M. Borlaf, L. Conti, K. Florio, M. Vetterli, T. Graule, M. Schmid, K. Wegener, Laser-based powder bed fusion of alumina toughened zirconia, Addit. Manuf. 31 (2020) 100959, http://dx.doi.org/10.1016/j.addma.2019.100959.
[125] A. Pesce, A. Hornés, M. Núñez, A. Morata, M. Torrella, A. Tarancón, 3D printing the next generation of enhanced solid oxide fuel and electrolysis cell, J. Mater. Chem. A 8 (2020) 16926, http://dx.doi.org/10.1039/d0ta02803g.
[126] J.C. Ruiz-Morales, A. Tarancón, J. Canales-Vázquez, J. Méndez-Ramos, L. Hernández-Afonso, P. Acosta-Mora, J.R. Marín-Rueda, R. Fernández-González, Three dimensional printing of components and functional devices for energy and environmental applications, Energy Environ. Sci. 10 (2017) 846, http://dx.doi.org/10.1039/c6ee03526d.
[127] R.I. Merino, J.I. Peña, M.A. Laguna-Bercero, A. Larrea, V.M. Orera, Directionally solidified calcia stabilised zirconia–nickel oxide plates in anode supported solid oxide fuel cells, J. Eur. Ceram. Soc. 24 (2004) 1349–1353, http://dx.doi.org/10.1016/S0955-2219(03)00562-4.
[128] R.I. Merino, J.I. Peña, V.M. Orera, Compositionally graded YSZ-NiO composites by surface laser melting, J. Eur. Ceram. Soc. 30 (2) (2010) 147–152, http://dx.doi.org/10.1016/j.jeurceramsoc.2009.04.031.
[129] G. Garcia, R.I. Merino, V.M. Orera, A. Larrea, J.I. Peña, M.A. Laguna-Bercero, J.A. Pardo, J. Santiso, A. Figueras, YSZ thin films deposited on NiO-CSZ anodes by pulsed injection MOCVD for intermediate temperature SOFC applications, Chem. Vap. Deposition 10 (2004) 249–252, http://dx.doi.org/10.1002/cvde.200304173.
[130] R. Campana, A. Larrea, J.I. Peña, V.M. Orera, Ni-YSZ cermet micro-tubes with textured surface, J Eur. Ceram. Soc. 29 (2009) 85–90, http://dx.doi.org/10.1016/j.jeurceramsoc.2008.06.005.
[131] A. Cubero, J.I. Peña, M.A. Laguna-Bercero, Optimization of Ni-YSZ solid oxide fuel cell anodes by surface laser melting, Appl. Surf. Sci. 335 (2015) 39, http://dx.doi.org/10.1016/j.apsusc.2015.01.230.
[132] Z. Fan, Y. Zhao, Q. Tan, B. Yu, M.X. Zhang, H. Huang, New insights into the growth mechanism of 3D-printed Al_2O_3–$Y_3Al_5O_{12}$ binary eutectic composites, Scr. Mater. 178 (2020) 274–280, http://dx.doi.org/10.1016/j.scriptamat.2019.11.040.
[133] P.B. Oliete, M.J. López-Robledo, J.I. Peña, J. Silva, Directionally solidified Al_2O_3–$ME_3Al_5O_{12}$ (ME: Y, Er and Yb) eutectic coatings for thermophotovoltaic systems, Ceram. Int.l 43 (2017) 16270–16275, http://dx.doi.org/10.1016/j.ceramint.2017.08.212.
[134] S.M. Eaton, H. Zhang, P.R. Herman, F. Yoshio, L. Shah, J. Bovatsek, A.Y. Arai, Heat accumulation effects in femtosecond laser-written waveguides with variable repetition rate, Opt. Express 13 (2005) 4708–4716, http://dx.doi.org/10.1364/OPEX.13.004708.
[135] A.V. Rode, B. Luther-Davies, E.G. Gamaly, Ultraast ablation with high-pulse-rate lasers. Part II: Experiments on laser deposition of amorphous carbon films, J. Appl. Phys. 85 (1999) 4222–4230, http://dx.doi.org/10.1063/1.370334.
[136] A.N. Samant, N.B. Dahotre, Laser machining of structural ceramics—a review, J. Eur. Ceram. Soc. 29 (2009) 969–993, http://dx.doi.org/10.1016/j.jeurceramsoc.2008.11.010.
[137] R. Lahoz, G.F. de la Fuente, J.M. Pedra, J.B. Carda, Laser engraving of ceramic tiles, Int. J. Appl. Ceram. Technol. 8 (2011) 1208–1217, http://dx.doi.org/10.1111/j.1744-7402.2010.02566.x.
[138] D. Fabris, A.F. Lasagni, M.C. Fredel, B. Henriques, Direct laser interference patterning of bioceramics: a short review, Ceramics 2 (2019) 578–586, http://dx.doi.org/10.3390/ceramics2040045.
[139] J. Berger, M. Grosse Holthaus, N. Pistillo, T. Roch, K. Rezwan, A.F. Lasagni, Ultraviolet laser interference patterning of hydroxyapatite surfaces, Appl. Surf. Sci. 257 (2011) 3081–3087, http://dx.doi.org/10.1016/j.apsusc.2010.10.120.
[140] S. Hermann, P. Engelhart, A. Merkle, T. Neubert, T. Brendemühl, R. Meyer, N.P. Harder, R. Brendel, 21.4%-Efficient emitter wrap-through rise solar cell on large area and picosecond laser processing of local contact openings, in: Proceedings of the 22nd European Photovoltaic Solar Energy Conference, Milan, Italy, 2007, pp. 970–975.
[141] G. Scotti, D. Trusheim, P. Kanninen, D. Naumenko, M. Schulz-Ruhtenberg, V. Snitka, T. Kallio, S. Franssila, Picosecond laser ablation for silicon micro fuel cell fabrication, J. Micromech. Microeng. 23 (2013) 055021, http://dx.doi.org/10.1088/0960-1317/23/5/055021.
[142] G. Scotti, P. Kanninen, V.-P. Matilainen, A. Salminen, T. Kallio, Stainless steel micro fuel cells with enclosed channels by laser additive manufacturing, Energy 106 (2016) 475–481, http://dx.doi.org/10.1016/j.energy.2016.03.086.
[143] A. Morán-Ruiz, K. Vidal, A. Larrañaga, R. Montero, M.I. Arriortua, Femtosecond laser micromachining of metallic/ceramic composite material for solid oxide fuel cell devices, Int. J. Hydrogen Energy 41 (2016) 17053–17063, http://dx.doi.org/10.1016/j.ijhydene.2016.07.122.
[144] Laser-Cell EU project: http://www.laser-cell.eu.
[145] S. Cuynet, A. Caillard, S. Kaya-Boussougou, T. Lecas, N. Semmar, J. Bigarré, P. Buvat, P. Brault, Membrane patterned by pulsed laser micromachining for proton exchange membrane fuel cell with sputtered ultra-low catalyst loadings, J. Power Source 298 (2015) 299–308, http://dx.doi.org/10.1016/j.jpowsour.2015.08.019.
[146] M. Navarro, B. Seoane, E. Mateo, R. Lahoz, G.F. de la Fuente, J. Coronas, ZIF-8 micromembranes for gas separation prepared on laser-perforated brass supports, J. Mater. Chem. A2 (2014) 11177–11184, http://dx.doi.org/10.1039/C4TA00547C.
[147] W. Dong, K. Wang, J. Han, Y. Yu, G. Liu, C. Li, P. Tong, W. Li, C. i Yang, Z. Lu, Regulating lithium electrodeposition with laser-structured current collectors for stable lithium metal batteries, ACS Appl. Mater. Interfaces 13 (2021) 8417–8425, http://dx.doi.org/10.1021/acsami.0c21301.
[148] J. Park, C. Jeon, W. Kim, S.-J. Bong, S. Jeong, H.-J. Kim, Challenges, laser processing and electrochemical characteristics on application of ultra-thick electrode for high-energy lithium-ion battery, J. Power Source 482 (2021) 228948, http://dx.doi.org/10.1016/j.jpowsour.2020.228948.
[149] W. Pfleging, Recent progress in laser texturing of battery materials: a review of tuning electrochemical performances, related material development, and prospects for large-scale manufacturing, Int. J. Extrem. Manuf. 3 (2021) 012002, http://dx.doi.org/10.1088/2631-7990/abca84.
[150] J. Proell, R. Kohler, A. Mangang, S. Ulrich, C. ZIiebert, W. Pfleging, 3D structures in battery materials, J. Laser Micro Nanoeng 7 (1) (2012) 97–104, http://dx.doi.org/10.2961/jlmn.2012.01.0019.
[151] C. Xu, Q. Li, Q. Wang, X. Kou, H.-T. Fang, L. Yang, Femtosecond laser drilled micro-hole arrays in thick and dense 2D nanomaterial electrodes toward high volumetric capacity and rate performance, J. Power Source 492 (2021) 229638, http://dx.doi.org/10.1016/j.jpowsour.2021.229638.

[152] M.R.H. Knowles, G. Rutterford, D. Karnakis, A. Ferguson, Micro-machining of metals, ceramics and polymers using nanosecond lasers, Int. J. Adv. Manuf. Technol. 33 (2007) 95–102, http://dx.doi.org/10.1007/s00170-007-0967-2.
[153] D. Sola, J. Gurauskis, J.I. Peña, V.M. Orera, Cold laser machining of nickel-yttrium stabilised zirconia cermets: composition dependence, Mat. Res. Bull. 44 (2009) 1910–1915, http://dx.doi.org/10.1016/j.materresbull.2009.05.006.
[154] J. Gurauskis, D. Sola, J.I. Peña, V.M. Orera, Laser drilling of Ni-YSZ cermets, J. Eur. Ceram. Soc. 28 (2008) 2673–2680, http://dx.doi.org/10.1016/j.jeurceramsoc.2008.04.012.
[155] S. Tsochataridou, G.A. Mutch, D. Neagu, E.I. Papaioannou, M.L. Sanjuán, B. Ray, R.I. Merino, V.M. Orera, I.S. Metcalfe, ACS Appl. Mater. Interfaces 12 (2020) 16436–16441, http://dx.doi.org/10.1021/acsami.0c01047.
[156] A. Larrea, D. Sola, M.A. Laguna-Bercero, J.I. Peña, R.I. Merino, V.M. Orera, Self-supporting thin yttria-stabilised zirconia electrolytes for solid oxide fuel cells prepared by laser machining, J. Electrochem. Soc. 158 (2011) B1193, http://dx.doi.org/10.1149/1.3619759.
[157] N.Q. Minh, Ceramic fuel cells, J. Amer. Ceram. Soc. 76 (1992) 563–588, http://dx.doi.org/10.1111/j.1151-2916.1993.tb03645.x.
[158] J.A. Cebollero, R. Lahoz, M.A. Laguna-Bercero, J.I. Peña, A. Larrea, V.M. Orera, Characterization of laser-processed thin ceramic membranes for electrolyte-supported solid oxide fuel cells, Int. J. Hydrog. Energy 42 (19), 13939–13948, doi:10.1016/j.ijhydene.2016.12.112.
[159] D. Sola, A. Escartín, R. Cases, J.I. Peña, Laser ablation of advanced ceramics and glass-ceramic materials: reference position dependence, Appl. Surf. Sci. 257 (2011) 5413–5419, http://dx.doi.org/10.1016/j.apsusc.2010.09.089.
[160] D. Sola, J.I. Peña, Study of the wavelength dependence in laser ablation of advanced ceramics and glass-ceramic materials in the nanosecond range, Materials 6 (2013) 5302–5313, http://dx.doi.org/10.3390/ma6115302.
[161] S.B. Adler, Factors governing oxygen reduction in solid oxide fuel cell cathodes, Chem. Rev. 104 (2004) 4791–4843, http://dx.doi.org/10.1021/cr020724o.
[162] J. Mizusaki, H. Tagawa, K. Tsuneyoshi, A. Sawata, Reaction kinetics and microstructure of the solid oxide fuel cell air electrode $La_{0.6}Ca_{0.4}MnO_3$/YSZ, J. Electrochem. Soc. 138 (1991) 1867–1873, http://dx.doi.org/10.1149/1.2085891.
[163] D. Herbstritt, A. Weber, E. Ivers-Tiffee, Modelling and DC-polarisation of a three dimensional electrode/electrolyte interface, J. Eur. Ceram. Soc. 21 (2001) 1813–1816, http://dx.doi.org/10.1016/s0955-2219(01)00121-2.
[164] D. Ding, X.X. Li, S.Y. Lai, K. Gerdes, M.L. Liu, Enhancing SOFC cathode performance by surface modification through infiltration, Energy Environ. Sci. 7 (2014) 552–575, http://dx.doi.org/10.1039/c3ee42926a.
[165] H. Shimada, K. Takizawa, H. Michibata, A. Hagiwara, M. Ihara, Equivalent circuit model analysis of microstructure-controlled LSM/ScSZ composite cathodes by powder slurry impregnation method, J. Electrochem. Soc. 162 (2015) F40–F53, http://dx.doi.org/10.1149/2.0211501jes.
[166] C.-C. Chao, C.-M. Hsu, Y. Cui, F.B. Prinz, Improved solid oxide fuel cell performance with nanostructured electrolytes, ACS Nano. 5 (2011) 5692–5696, http://dx.doi.org/10.1021/nn201354p.
[167] M. Motoyama, C.C. Chao, J.H. An, H.J. Jung, T.M. Gur, F.B. Prinz, Nanotubular array solid oxide fuel cell, ACS Nano. 8 (2014) 340–351, http://dx.doi.org/10.1021/nn4042305.
[168] W.Z. Zhu, S.C. Deevi, A review on the status of anode materials for solid oxide fuel cells, Mater. Sci. Eng. A-Struct. Mater. Prop. Microstruct. Process. 362 (2003) 228–239, http://dx.doi.org/10.1016/s0921-5093(03)00620-8.
[169] T. Ryll, H. Galinski, L. Schlagenhauf, P. Elser, J.L.M. Rupp, A. Bieberle-Hutter, L.J. Gauckler, Microscopic and nanoscopic three-phase-boundaries of platinum thin-film electrodes on YSZ electrolyte, Adv. Funct. Mater. 21 (2011) 565–572, http://dx.doi.org/10.1002/adfm.201001729.
[170] X.-M. Wang, C.-X. Li, J.-Y. Huang, G.-J. Yang, C.-J. Li, Deposition mechanism of convex YSZ particles and effect of electrolyte/cathode interface structure on cathode performance of solid oxide fuel cell, Int. J. Hydrogen Energy. 39 (2014) 13650–13657, http://dx.doi.org/10.1016/j.ijhydene.2014.04.117.
[171] F. Tsumori, Y. Tanaka, Y. Xu, T. Osada, H. Miura, Development of improved solid oxide fuel cell electrolyte sheet by microimprinting for layered material, Jpn. J. Appl. Phys. 53 (2014), http://dx.doi.org/10.7567/jjap.53.06jk02.
[172] H. Seo, H. Iwai, M. Kishimoto, C. Ding, M. Saito, H. Yoshida, Microextrusion printing for increasing electrode–electrolyte interface in anode-supported solid oxide fuel cells, J. Power Sources 450 (2020) 227682, http://dx.doi.org/10.1016/j.jpowsour.2019.227682.
[173] J.A. Cebollero, R. Lahoz, M.A. Laguna-Bercero, A. Larrea, Tailoring the electrode-electrolyte interface of Solid Oxide Fuel Cells (SOFC) by laser micro-patterning to improve their electrochemical performance, J. Power Sources 360 (2017) 336–344, http://dx.doi.org/10.1016/j.jpowsour.2017.05.106.
[174] J.A. Cebollero, M.A. Laguna-Bercero, R. Lahoz, J. Silva, R. Moreno, A. Larrea, Optimization of laser-patterned YSZ-LSM composite cathode-electrolyte interfaces for solid oxide fuel cells, J. Eur. Ceram. Soc. 39 (2019) 3466–3474, http://dx.doi.org/10.1016/j.jeurceramsoc.2019.02.049.
[175] M. Kishimoto, H. Iwai, M. Saito, H. Yoshida, Quantitative evaluation of solid oxide fuel cell porous anode microstructure based on focused ion beam and scanning electron microscope technique and prediction of anode overpotentials, J. Power Sources 196 (2011) 4555–4563, http://dx.doi.org/10.1016/j.jpowsour.2010.12.100.
[176] H. Seo, H. Iwai, M. Kishimoto, M. Saito, H. Yosida, R. Lahoz, M.A. Laguna-Bercero, A. Larrea, Extension of effective reaction region in anode-supported SOFCs using pulse laser processing, 56th Natl. Heat Transf. Symp. Jpn. (2019).